Chemical Engineering Journal 372 (2019) 429–451

Contents lists available at ScienceDirect

Chemical Engineering Journal

journal homepage: www.elsevier.com/locate/cej

Review

Surfactant-assisted synthesis of photocatalysts: Mechanism, synthesis, recent advances and environmental application

Qinghua Liang[a,1], Xiaojuan Liu[b,1], Guangming Zeng[a,1], Zhifeng Liu[a,*], Lin Tang[a,*], Binbin Shao[a], Zhuotong Zeng[c], Wei Zhang[b], Yang Liu[a], Min Cheng[a], Wangwang Tang[a], Shanxi Gong[d]

[a] College of Environmental Science and Engineering, Hunan University and Key Laboratory of Environmental Biology and Pollution Control (Hunan University), Ministry of Education, Changsha 410082, PR China
[b] The First Affiliated Hospital of Hunan University of Chinese Medicine, Changsha 410007, China
[c] Department of Dermatology, Second Xiangya Hospital, Central South University, Changsha 410011, Hunan, PR China
[d] School of Chemistry and Chemical Engineering, Guangxi University, Nanning 530004, PR China

HIGHLIGHTS

- Surfactant-assisted synthesis is a promising method for photocatalyst synthesis.
- Surfactant would efficiently enhance the photocatalytic activity of photocatalysts.
- Surfactant can regulate the morphology and structure of photocatalysts.
- Influencing factors and recent advances are highlighted.

GRAPHICAL ABSTRACT

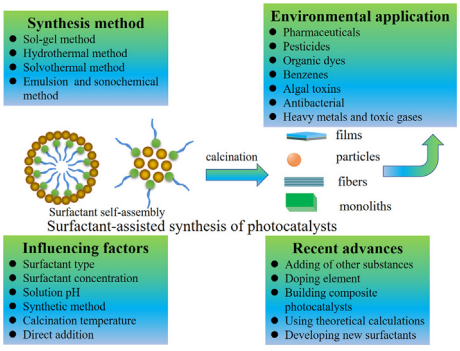

ARTICLE INFO

Keywords:
Surfactant
Self-assembly
Photocatalyst
Environmental remediation
Photocatalytic degradation

ABSTRACT

The presence of large amounts of contaminants in the environment would result in ecological and health hazards. The photocatalytic technologies have been developed to use sunlight to remove contaminants in recent years. Researchers are primarily focused on developing high-performance photocatalysts. This review discusses the effects of surfactant on the structural morphology, physicochemical properties and contaminant removal performance of photocatalysts. The mechanism and synthesis method of surfactant-assisted photocatalysts are reviewed. Meanwhile, the effects of surfactant type, surfactant concentration, solution pH, synthesis method and calcination temperature on the photocatalysts are also discussed in detail. In addition, we summarized the recent advances and the application of surfactant-assisted photocatalysts in the environmental remediation. Finally, the future researches on surfactant-assisted photocatalysts are also proposed. This review provides new insights into the use of surfactants to prepare photocatalysts with well-defined shape and excellent performance to enhance photocatalytic efficiency for removing pollutants.

* Corresponding authors.
E-mail addresses: zhifengliu@hnu.edu.cn (Z. Liu), tanglin@hnu.edu.cn (L. Tang).
[1] The authors contribute equally to this paper.

https://doi.org/10.1016/j.cej.2019.04.168
Received 25 February 2019; Received in revised form 23 April 2019; Accepted 24 April 2019
Available online 25 April 2019

1. Introduction

More and more pollutants are being discharged into the air, water, and soil over the past few years due to the development of industry [1–3], which could cause irreversible damage to the environment and human [4–6]. The environmental pollution has become an urgent problem that both government and general public have to face in the present situation. A lot of researches have been focused on the technologies of removing pollutants from wastewater, such as adsorption, biodegradation, reverse osmosis, flocculation, electrochemical oxidation, and photocatalysis [7–12].

In recent decades, the photocatalytic technology was regarded as an effective technique to solve water pollution problems, which utilizes sunlight to turn contaminants into mineral salts and final products, such as CO_2 and H_2O [13–15]. This technology has attracted increasing attention during the past few decades due to its advantages of low cost, high efficiency and sustainable treatment [16–18]. Various photocatalytic materials, such as TiO_2, Cu_2O, BiOCl, WO_3, and CdS, can be used as photocatalysts to degrade pollutants [19–22]. However, most photocatalytic materials have some disadvantages, such as low utilization efficiency of visible light and fast recombination of electron and hole pairs, resulting in low catalytic efficiency [23–25]. Therefore, it is necessary to modify photocatalyst to increase the photocatalytic performance for contaminants degradation. The modification technologies of photocatalysts, including constructing heterojunctions, building built-in electric fields, doping elements, and introducing photosensitizers, etc., have been reported in many literatures [26–29]. It is worth noting that the photocatalysts with well-structured and morphology, such as core-shell structure, uniform spherical and hierarchical multilayer structure, can favor the electronic transfer, and enhance optical absorption and photocatalytic performance [30–32]. Therefore, how to prepare a photocatalyst with well-structured and morphology is a crucial issue.

There are increasing interests in surfactant-assisted mesoporous materials since the mesoporous silicate MCM-41 was successfully synthesized [33–35]. Surfactants are an amphiphilic substance with hydrophilic and hydrophobic groups, which has been proven to be a good shape-directing agent in the synthesis of photocatalysts, controlling their overall shape primarily by adsorption of surface active molecules on different crystal faces of the nucleation center [36–38]. Initially, surfactants were used to regulate the growth of single crystal photocatalysts particles, such as TiO_2 [39], WS_2 [40], BiOCl [41], $BiVO_4$ [42]. With the continuous development, surfactants have received more and more attention in the regulation of composite materials, such as N-doped $Bi_2O_2CO_3$ [43], and BiOBr/Bi [44]. The hydrophobic groups of the surfactant molecule adsorb on the charged surface of the photocatalyst by some non-covalent interactions, such as hydrogen bonding, π-π interaction, and van der Waals interaction, while the hydrophilic groups are in contact with water in aqueous solution. This adsorption is usually selective on a particular crystal plane because the nucleation center is predominantly a tiny polyhedral morphology. Consequently, this adsorption results in an ordered shape evolution. The addition of a surfactant during the preparation of the photocatalysts not only induces the photocatalysts to expose highly active lattice surface, but also induces the photocatalyst to have the characteristics of the ordered structure, abundant pores, and large surface area. These changes improve the physicochemical properties of the photocatalyst, thereby increasing the photocatalytic performance [45–47].

In the case of surfactant-assisted synthesis of photocatalysts, many influencing factors have been studied to obtain photocatalysts with high catalytic performance, including surfactant type, surfactant concentration, solution pH, synthesis method, and calcination temperature, etc. [7,48,49]. To the best of our knowledge, only a few reviews have reported surfactant-related work, which were focused on the direct addition of surfactants as solubilizers or extractants to improve contaminant removal by photocatalysts [5,50–52] or the effects of surfactants in the synthesis of nanomaterials [36,53] (such as controlling the shape of materials, preparing layered porous materials). It is important to collect information on this topic to understand the effect of surfactants on the crystal structure and physicochemical properties of the photocatalysts. In this review, we focus on an overview of the mechanisms of action, preparation conditions, recent advances, and environmental applications of surfactant-assisted synthesis of photocatalysts, which is supposed to help to understand and design photocatalysts.

2. Action mechanism and synthesis method

The mechanisms of photocatalysts prepared by surfactants are complex, and many articles have reported them [54,55]. It is generally believed that due to the non-covalent interactions, such as hydrogen bonding, π-π interaction, and van der Waals interaction, between the surfactant and solid material, the surfactant was adsorbed on the surface of the solid material, inducing the material to self-assemble. At the same time, surfactants acted as active agents to reduce the interfacial force between the nanocrystals and water during self-assembly [56]. In addition, the encapsulation of the surfactant micelles was thermodynamically beneficial to further self-assembly of the photocatalysts. Finally, the photocatalysts with an ordered structure and a well-defined shape were formed.

The formation process of surfactant-assisted synthesis of photocatalysts can be generally divided into two steps of hydrolysis and polymerization [53,54]. In the first stage, the precursor solution is hydrolyzed in preparation for the formation of the sol. In the second stage, a single surfactant molecule is bound by adsorption of the head and the hydrolyzed solid surface according to the interaction force. Then the surfactant strongly promotes adsorption through the hydrophobic interaction between the tail groups. The nanocomposite formed at this time is called a colloidal particle (otherwise known as sol). These colloidal particles then aggregate to form the gel due to mutual attraction. Finally, the gel is passed through a heat treatment to remove the surfactant to give the final shape of the photocatalyst. It is worth noting that during crystal growth, the evolution of the shape is controlled by the surface energy of each face, and the crystal tends to grow rapidly on the surface with high surface energy [57].

However, the mechanism of the surfactant-assisted synthesis of photocatalysts is slightly different with different preparation methods. Therefore, we summarize the mechanism in combination with the synthesis method and analyze them by the reaction process reported in literature. Surfactant-assisted photocatalysts have been synthesized through various techniques, which mainly include sol-gel method, hydrothermal method, solvothermal method, emulsion method, and sonochemical method, etc. Among them, the most common synthesis methods are the sol-gel method, hydrothermal method, and solvothermal method. The sol-gel and hydrothermal methods are used in an aqueous media, whereas the solvothermal employs a non-aqueous media for the reaction.

2.1. Sol-gel method

The sol-gel method has the advantages of high stability, short soaking times, low reaction temperature and high purity of products, and it is considered to be one of the most promising methods for synthetic photocatalysts. In addition, the photocatalysts particles prepared by the sol-gel process generally have a narrow and uniform distribution and thermal stability. Therefore, the sol-gel method has attracted much attention in the preparation of porous photocatalysts [58]. This approach has been successful in the controllable design of multi-dimensional photocatalysts, such as pellets, fibers, films, and blocks.

The chemical reactions involved in the sol-gel process are based on inorganic polymerization. As shown in Fig. 1, the preparation process of the method is divided into three steps, namely hydrolysis,

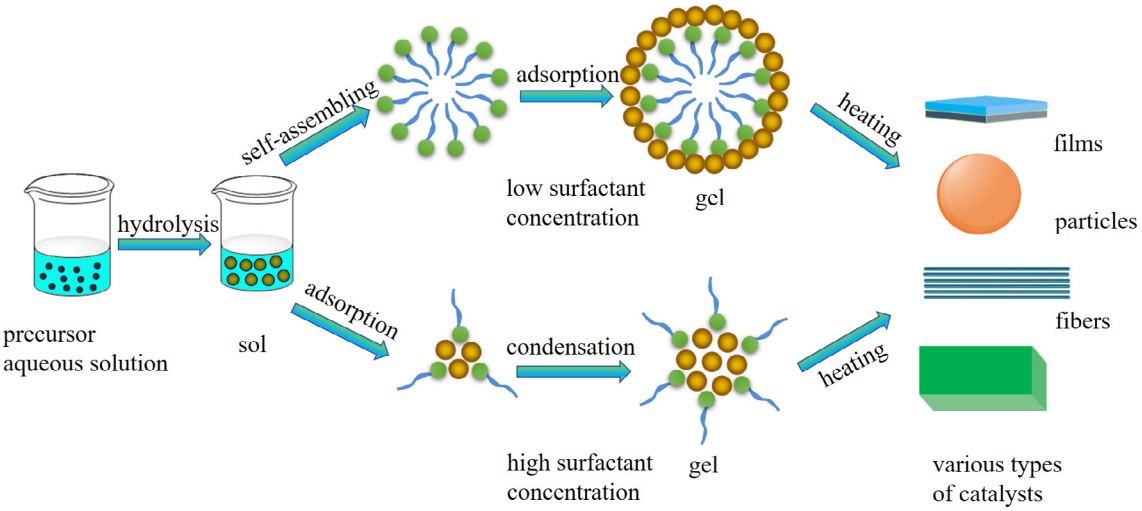

Fig. 1. The possible preparation process of surfactant-assisted photocatalysts by sol-gel method. Modified with permission from Ref. [60]. Copyright 2014 Elsevier.

polymerization and gel drying. Firstly, a solution of the precursor molecules needs to be hydrolyzed. The precursor is typically a metal organic compound such as an alkoxide, a chelated alkoxide or a metal salt. After hydrolysis, a suspension of colloidal particles (sol) is formed. Secondly, a large amount of water is present in the sol, and during the gelation process, the system loses fluidity and forms an open skeleton structure (gel). Finally, the gel is calcined to remove the surfactant to obtain the final photocatalyst [53,59].

For example, cetyltrimethylammonium bromide (CTAB) acted as a surfactant and self-assembles into spherical vesicles in an ethanol-water solution (Fig. 1) [60]. Studies found that the rate of hydrolysis of the precursor tetraethyl orthosilicate (TEOS) increased with the concentration of CTAB. Therefore, the increase of the CTAB concentration resulted in a faster nucleation rate than the CTAB self-assembly rate, which formed bioactive glass (BG) sol particles firstly. Then, CTAB was adsorbed to the surface of the BG sol particles by hydrogen bonding interaction. Finally, CTAB was removed to obtain a solid mesoporous BG sphere after calcination. Conversely, when the concentration of CTAB was low, the rate of CTAB self-assembly was greater than that of nucleation, resulting in the self-assembly of CTAB molecules into spherical vesicles. The BG sol was then adsorbed to the surface of the vesicle by hydrogen bonding interaction. Finally, the hollow mesoporous BG sub-micron spheres (HMBGS) photocatalysts were obtained after calcination.

2.2. Hydrothermal method

Although the sol-gel method is widely used in the preparation of photocatalysts, the cost is high due to the requirement of expensive precursors and solvents. Therefore, another synthesis method, the hydrothermal method has also been studied. Compared with other crystal preparation methods, the photocatalysts prepared by the hydrothermal method have the advantages of good grain development, small particle size, uniform distribution, and low-cost raw photocatalysts. In particular, they have the unique advantages of high crystallinity and morphology control [61]. The hydrothermal method has been successful in the controllable design of multi-dimensional photocatalysts, such as 1D photocatalysts (nanowires, nanobelts, nanotubes), hollow and thin films.

In general, the hydrothermal method uses water as a solvent, and the sample needs to be dissolved and recrystallized firstly [62]. The possible preparation process of the hollow structure is shown in Fig. 2. The sample is mixed in a solution and the reaction is carried out at a certain temperature. During the period, due to the presence of the surfactant, the samples self-assemble to form fine particles, and as the

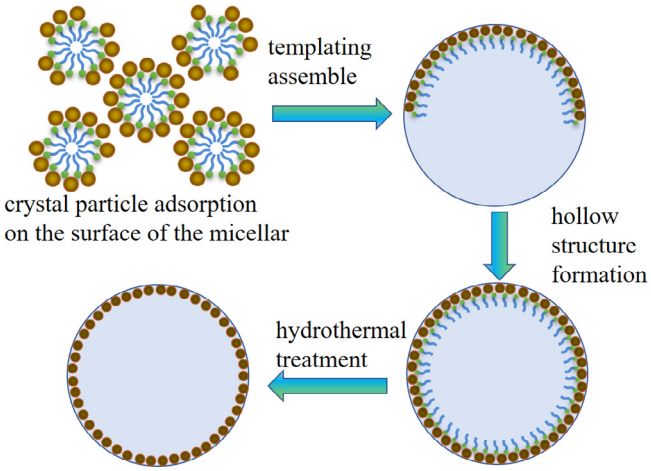

Fig. 2. The possible preparation process of hollow photocatalysts by hydrothermal method. Modified with permission from Ref. [61]. Copyright 2013 Elsevier.

crystal grains grow up, the final morphology products are obtained. For example, in the preparation of hierarchically mesoporous titanium phosphonates (HM-TiPPh), a cationic surfactant CTAB and an anionic polymer poly (acrylic acid) (PAA) were added [31]. Firstly, assembled particulars occurred between CTAB micelles and PAA due to differences in charge properties. PAA led to the formation of a highly ordered mesophase and mesogenic PAA-CTAB complex by electrostatic interaction, in which a negatively charged phosphonic acid group was also involved in the supramolecular complex. After the addition of the active substance $TiCl_4$, the hydrolysis and polymerization between $TiCl_4$ and the phosphonic acid group produced an electronegative titanium phosphonate oligomer, which reduced the electrostatic interaction between CTAB and PAA. That resulted in the reassembly of the intermediate phase. Around the CTAB micelles, the titanium phosphonate material was crosslinked with the ordered mesogen complex to give an ordered mesostructure. In addition, the electrostatic interaction between the PAA and CTAB micelles was disturbed, resulting in the separation of some PAA chains from the mesomorphic complex and forming a phase separated PAA chain domain, and it served as a template for the formation of interstitial pores inside the sphere.

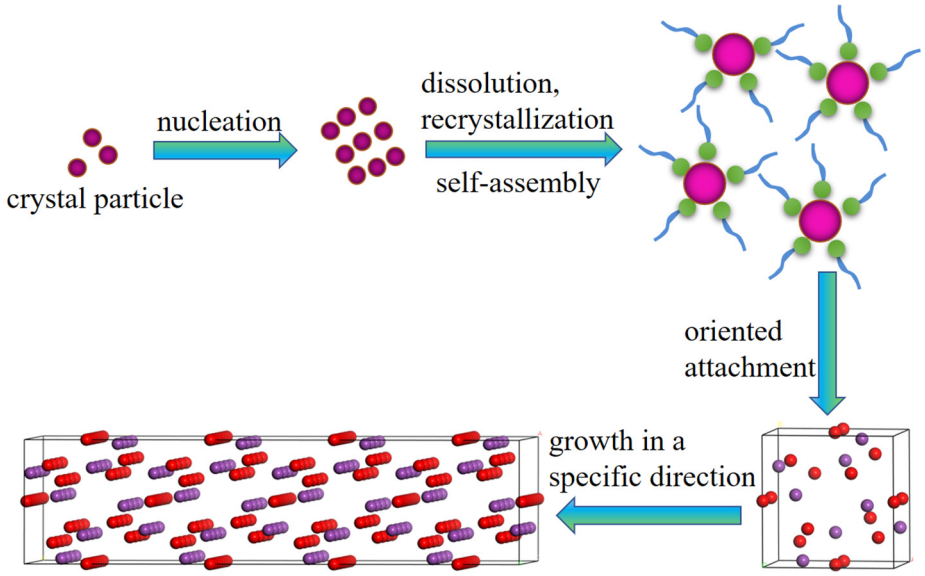

Fig. 3. The possible preparation process of surfactant-assisted photocatalysts by solvothermal method. Modified with permission from Ref. [64]. Copyright 2014 American Chemical Society.

2.3. Solvothermal method

The solvothermal method is developed on the basis of the hydrothermal method, using an organic or non-aqueous solvent as a solvent and the mixture reacting at a certain temperature [63,64]. The hydrothermal method is commonly used to the preparation of oxide photocatalysts or some water-insensitive sulfur-containing compounds, while the preparation of some water-sensitive compounds such as III–V semiconductors, carbides, fluorides, and other photocatalysts are not applicable. Compared with the hydrothermal method, the solvothermal method uses a non-aqueous solvent, which expands the range of solvent-based raw materials [65].

It is worth noting that, unlike the sol-gel and hydrothermal methods, the process of solvothermal preparation of photocatalysts is mainly divided into nucleation, dissolution, recrystallization, and growth (Fig. 3). The preparation process of SnS_2 photocatalysts by the solvothermal method was as follows [64]: firstly, the thioacetamide (TAA) was decomposed during the heat treatment and produced S^{2-}. Then, Sn^{2+} and S^{2-} rapidly nucleated to form SnS microfluidics. Subsequently, the SnS_2 core was formed as the reaction proceeds due to the excess of the S source, in which a process of dissolution-recrystallization growth might be experienced. The surface energy of the side of SnS_2 was higher than the surface of the nanosheet, resulting in the formation of a new layer on the surface. However, due to the high density of the (0 0 1) plane, this provided a small interatomic distance and great binding. Therefore, atoms would be more easily adsorbed on the (0 0 1) facets for growth. Polyvinylpyrrolidone (PVP) molecules adsorbed on the (0 0 1) facet inhibited the crystal growth along (0 0 1). Therefore, a regular and uniform SnS_2 nanosheet was finally obtained.

2.4. Other synthesis methods

In addition to the above three commonly used synthesis methods, other synthesis methods have also been reported in the surfactant-assisted synthesis of photocatalysts, such as emulsion polymerization and sonochemical methods.

2.4.1. Emulsion method

The emulsion polymerization method is a method in which a monomer is dispersed in water by an emulsifier and mechanical stirring to form an emulsion, and an initiator is added to initiate polymerization of the monomer. The emulsion polymerization has the characteristics of high polymerization speed, high reaction conversion rate, low viscosity, stable dispersion system, and easy control. However, the separation and precipitation process of the polymer obtained by the emulsion polymerization method is complicated, and a demulsifier or a coagulant is added so that there are many residual impurities in the product. In addition to conventional emulsion polymerization, reverse emulsion polymerization, soap-free emulsion polymerization, microemulsion polymerization, dispersion polymerization, and so on are also included. We mainly introduce the oil-in-water and water-in-oil emulsion polymerization.

Conventional emulsion polymerization refers to an aqueous monomer solution prepared from a water-soluble monomer which forms an oil-in-water emulsion with an organic phase under the action of an oil-soluble surfactant [66]. In contrast to emulsion polymerization, the inverse emulsion polymerization forms a water-in-oil emulsion [67]. The reaction mechanism of the two methods is similar. The polymerization mechanism can be divided into four stages: dispersion stage, aggregation stage, growth stage, and polymerization completion stage. The possible synthesis process of the emulsion polymerization process is shown in Fig. 4.

There are also some papers reporting the use of emulsion polymerization in surfactant-assisted photocatalysis. Zhu et al. synthesized Ag/AgBr/GO by a water-in-oil microemulsion method and oil-in-water microemulsion method, using CATB as surfactant, and studied its photocatalytic degradation effect on methyl orange [68]. In the water-in-oil microemulsion system, the hydrophobic alkyl chain of CTAB dissolves and points to the core of the organic phase chloroform. The polar head group of CTAB ($–N(CH_3)_3$) and Br^- dissolve and point to the aqueous phase, resulting in the production of AgBr. Because the component Br comes from the oil phase, and it is dispersed in the aqueous phase. Therefore, the surface of the formed AgBr is mainly terminated by Ag. In the water-in-oil microemulsion system, Ag is derived from the aqueous phase and dispersed in the oil phase. The component Br is derived from the body oil phase, which is dispersed in the aqueous phase. As a result, the surface of the formed Ag/AgBr is mainly terminated by Br. Therefore, the Ag/AgBr photocatalytic activity obtained in the water-in-oil microemulsion system is higher compared to that of oil-in-water microemulsion system.

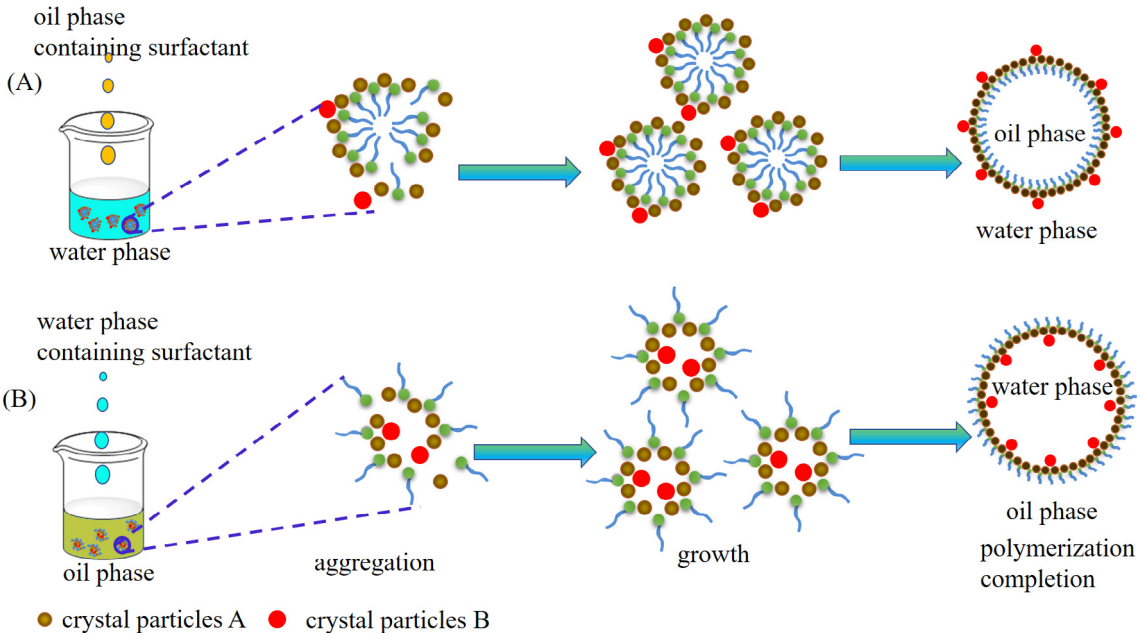

Fig. 4. The possible preparation process of surfactant-assisted photocatalysts by emulsion (A) water-in-oil, (B) oil-in-water polymerization method.

2.4.2. Sonochemical method

The sonochemical method is a method of accelerating chemical reactions using ultrasonic waves. The sonochemical reaction is mainly caused by acoustic cavitation – the formation, oscillation, growth, shrinkage, and collapse of liquid hollow bubbles. This method has become an important tool for the production of novel nano-sized materials under ambient conditions in synthetic chemistry [69,70]. Compared with the sol-gel method, hydrothermal method, solvothermal, etc., the sonochemical method has the advantages that the reaction temperature is low and the high temperature is not required. According to the hotspot theory, local hot spots can reach extremely high temperatures (> 5000 K) when bubbles burst, and these extreme conditions can be used to synthesize a variety of materials. The mechanism of the sonochemical method is relatively complicated. It is generally believed that water decomposes into hydroxyl radicals and hydrogen under the action of ultrasonic waves, thereby triggering a series of chemical reactions.

There are few articles reporting the application of the sonochemical method in surfactant-assisted photocatalysts. Panahi-Kalamuei et al. synthesized nano-selenium (Se) by the sonochemical method and studied the effects of various surfactants on the material [71]. The results of characterization indicate that lowering the vapor pressure of the solvent results in an increase in cavitation collapse strength. Therefore, the rate of sonochemical reaction increases due to reaching a peak temperature during the collapse. In this work, the use of water and surfactants with different vapor pressures and viscosities affects the particle size of the material because solvent vapors can indirectly affect the chemical reaction rate. In addition, according to the degradation experiment results, the photocatalyst prepared by different surfactants showed different photocatalytic degradation properties for methyl orange.

3. Influencing factors on the performance of surfactant-assisted synthesis of photocatalysts

In the process of surfactant-assisted synthesis of photocatalyst, the structure and morphology of the photocatalysts are mainly controlled by numerous parameters. As shown in Fig. 5, it can be divided into five categories: surfactant type, surfactant concentration, solution pH, synthesis method, and calcination temperature [7,72,73], and the surfactant-assisted photocatalysts, shapes, and mechanism with different influencing factors are shown in Table 1.

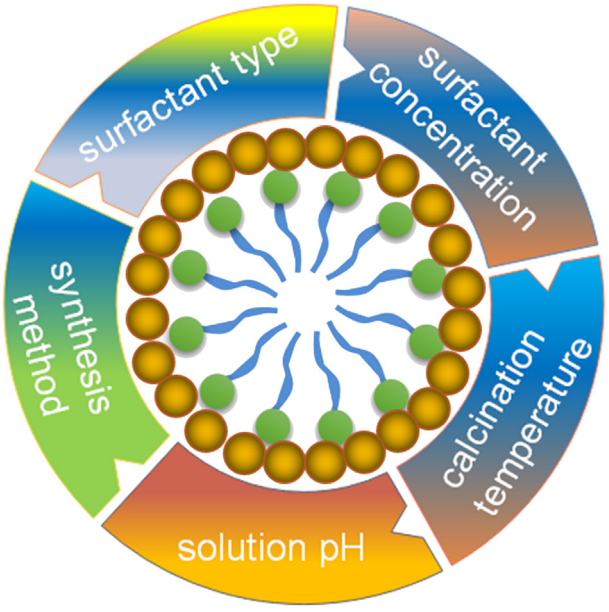

Fig. 5. Influencing factors on surfactant-assisted synthesis of photocatalysts.

3.1. The effect of surfactant type

In the synthesis of photocatalysts, surfactant type plays a crucial role, which has been used for shape-controlled of photocatalysts [74–76]. The type of surfactants mainly relates to the charge, shape, hydrophobic chain length, and functional groups of surfactants, and the possible reflection diagram is shown in Scheme 1.

3.1.1. The charge property of surfactant

According to the difference in the charge properties of the surfactants, surfactants can be classified into anionic surfactants, cationic surfactants, zwitterionic surfactant, and nonionic surfactants. The surfactant-assisted photocatalysts and shapes with different charge

Table 1
The surfactant-assisted photocatalysts, shapes and mechanisms with different influencing factors.

Influencing factor	Surfactant	Photocatalyst and shape	Conclusion and mechanism	Ref.
The charge property of surfactant	Cetyl trimethyl ammonium bromide (CTAB, cationic surfactant)	Gold nanocombs; linear and leaf-like particles	Different charge surfactants affect the structure of the photocatalyst due to electrostatic interaction and capping effect	[85]
	Sodium dodecyl sulfate (SDS, anionic surfactant)	Gold nanocombs; irregular star particles		
	CTAB-SDS mixed surfactant	Gold nanocombs; a clear gold nanobelt		
The shape of surfactant	CTAB	Zn_2SiO_4; uniform nanoparticles (10–55 nm)	The shape of the photocatalyst is related to the size and steric hindrance of the surfactant	[86]
	Polyvinylpyrrolidone (PVP)	Zn_2SiO_4; agglomerated products (60–300 nm)		
	SDS	Zn_2SiO_4; agglomerated products (200–400 nm)		
	Polyethylene glycol (PEG)	Zn_2SiO_4; irregular particals (60–300 nm)		
The length of the hydrophobic group of surfactant	Tris(trimethoxysilyloxy)-alkylsilanes	Silica-based hybrid mesostructures; ordered lamellar phases (n = 14–18)	The long alkyl chains form a strong hydrogen bond interaction with each other, resulting in the formation of a dense bilayer structure which limits the lateral growth of the crystal	[89]
		Silica-based hybrid mesostructures; two-dimensional (2D) hexagonal structures (n = 6–10)		
The functional group of surfactant	CTAB	Gold; short rod	This may be due to the additional non-polarity due to the presence of the benzyl ring, resulting in a mixed micet having a small micelle size	[91]
	CTAB and benzyldimethylhexadecylammonium chloride (BDAC, containing benzyl)	Gold; long and thin photocatalyst		
The effect of surfactant concentration	CTAC	Ag/AgCl/GO; spherical particles at low concentrations	The surfactant concentration affects the shape and structure of the catalyst	[94]
		Ag/AgCl/GO; cubic particles at high concentrations		
	PVP	α-Fe_2O_3; film; uniform and dispersion in high concentration	Surfactant concentration affects capping, combined with electrostatic repulsion or steric barrier interaction, affecting crystal growth	[93]
	CTAB	TiO_2; nanoparticles; as the amount of CTAB increased from 55 to 137 mM, the particle diameter of TiO_2 progressively decreased from 240 to 156 nm	The surfactant concentration affects the particle size of the photocatalyst by affecting surface tension and micelle self-assembly	[101]
	SDS	Nb_2O_5; nanorods; the intensity of the diffraction peak of the Nb_2O_5 at (1 1 0) planes initially increased and then decreased with the increase of SDS concentration	The high concentration of the surfactant hinders the growth of the crystal while increasing the defects of the catalyst and increasing the photocatalytic activity	[73]
The effect of solution pH	Myristyltrimethylammonium bromide (MTAB)	ZnTPP; nanoparticles, tetragonal nanorods, hexagonal porous nanodisks, and hexagonal nanorods	The shape of the photocatalyst also changed significantly as the pH changed. This is attributed to the fact that pH affects self-assembly behavior by affecting π-π stacking and coordination	[56]
	PVP	$BiVO_4$; nanorods, spherical	The crystal structure of the photocatalyst changes with the change of pH, which is due to the change of pH, which affects the interaction between ions and causes self-assembly to change	[42]
	CTAB	pH = 5–6, H_2GeO_4; nanorods	The pH of the solution affects the composition of the photocatalyst by affecting the hydrolysis of the material	[113]
		pH > 8, Zn_2GeO_4; nanorods		
The effect of synthetic method	Benzyl alcohol	TiO_2/MWCNTs; nanobelt; TiO_2 nanoparticles aggregated on the surface of the CNT in the sol-gel method	Different preparation methods affect the particle size, crystallinity and dispersion of the photocatalyst, which may be related to the reaction temperature	[115]
		The TiO_2 nanoparticles were uniformly decorated on the CNTs in the solvothermal method		
The effect of calcination temperature	Oleylamine	$ZnIn_2S_4$; nanosheets	The calcination temperature affects crystallinity, crystal size growth, and crystal form transformation of photocatalytic	[122]
	Benzyl alcohol	550 °C, anatase-TiO_2; 650 °C, anatase-TiO_2 and rutile-type TiO_2; 800 °C, rutile-type TiO_2		[123]
The effect of direct addition of surfactants in degradation solution	TritonX100 (TX100)	Bi_2WO_6	TX100 can pull the substrate molecule NOF near the surface of the photocatalyst by hydrophobic interaction. In addition, electron transfer between the semiconductor surface and the NOF is promoted by π-π interaction	[127]
	TX100	TiO_2	Increasing the solubility of phenanthrene in water significantly enhances the adsorption of phenanthrene on the surface of TiO_2	[129]

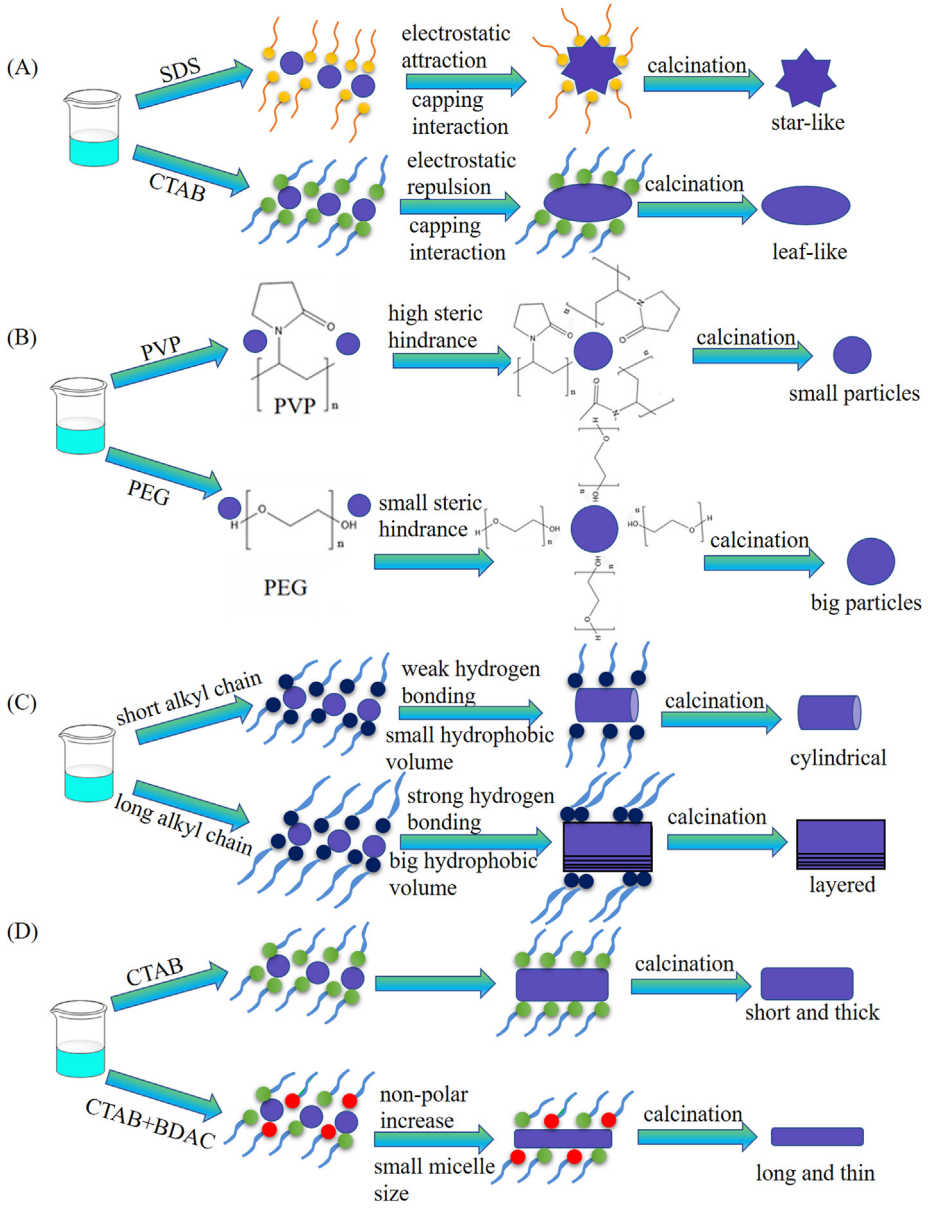

Scheme 1. Schematic diagram of the effect of the (A) charge, (B) shape, (C) alkyl chain length and (D) functional group of the surfactant on the size and morphology of the photocatalyst.

properties are shown in Table 2. Surfactants with different charge can act as a stabilizing agent, or dispersing agent, to control the size of the nanoparticles and minimizes agglomerations [77]. The nonionic surfactants can act as a dispersing agent to distribute the crystal evenly while increasing the active site and increasing electron transport [78,79]. Compared to nonionic surfactants, ionic surfactants usually exhibit clearer shape-directing effects [36]. The surface energy of crystal is changed with the presence of ionic surfactants, which is beneficial to the preferential growth of the crystal along the direction of surfactant absorbed [57,80,81]. The ratio of the (1 1 0)/(0 1 3) reflection was changed from 0.25 to 0.80, the size decreased from 40 nm to 10 nm, and the BET surface area increased from 7.9 $m^2 g^{-1}$ to 17.1 $m^2 g^{-1}$, after addition of ionic surfactant CTAB in the preparation of $Bi_2O_2CO_3$ nanosheet. Importantly, the photooxidation of NO was greatly improved from 6.7% to 30.4% in 5 min. Therefore, the addition of CTAB not only changed the structure and surface properties of the crystal through the interaction between the surfactant and the crystal but also affected the photocatalytic efficiency of the photocatalysts [43].

Due to the different properties of surfactants with different charges, a subtle control method of crystal growth in solution by mixing surfactants is proposed based on the cooperative effect between the mixed surfactants (Fig. 6A). Cationic/anionic mixed surfactants with different charge properties have been studied to regulate the morphological structure of crystals [82,83]. As shown in Fig. 6B–D, in the synthesis study of gold nanoribbons, when a single surfactant CTAB was used, linear and leaf-like particles were obtained at 4 °C, and irregular polyhedral particles were obtained at 27 °C. This may be due to electrostatic repulsion between cationic surfactants and positively charged gold ions, which results in the addition of positively charged surfactants promoting gold ion movement, thereby affecting crystal formation [84]. In addition, when a single surfactant sodium dodecyl sulfate (SDS) was used, irregular star particles were produced at 4 or 27 °C. This may be attributed to the electrostatic attraction between the anionic surfactant and the positively charged gold ions, which hinders the three-dimensional coordination, thereby affecting crystal formation. However, a clear gold nanobelt grown in two different directions was synthesized in an aqueous solution of the mixed surfactant. The adsorption of CTAB-

Table 2
The surfactant-assisted photocatalysts and shapes with different charge properties.

Photocatalyst	Surfactant	Charge property	Photocatalyst shape	Ref.
Gold nanocombs	Cetyltrimethylammonium bromide (CTAB) Sodium dodecyl sulfate (SDS)	Cationic surfactant Anionic surfactant	Linear and leaf-like particles Irregular star particles	[85]
Selenium	Polyethylene glycol (PEG) SDS CTAB	Nonionic surfactant Anionic surfactant Cationic surfactant	Smaller nanoparticles Smallest nanoparticles No product	[71]
$BiVO_4$	Hexadecyl trimethyl ammonium bromide (HTAB) Polyvinyl alcohol (PVA)	Cationic surfactant Nonionic surfactant	Microclusters Spherical	[196]
TiO_2	Sodium dodecyl benzene sulfonate (DBS) SDS Cellulose	Anionic surfactant Anionic surfactant Nonionic surfactant	Spherical Cubic Nanorods	[197]
Ag_2CrO_4 and $Ag_2Cr_2O_7$	SDS Polyethylene oxide (PEO)	Anionic surfactant Nonionic surfactant	Nanoparticles Regular nano-rods	[198]
$ZnIn_2S_4$	CTAB Cetylpyridinium bromide (CPBr) SDS	Cationic surfactant Cationic surfactant Anionic surfactant	Rose-like microclusters Loose rose-like Irregular rose-like	[199]
TiO_2	CTAB Polyethylene glycol (PEG)	Cationic surfactant Nonionic surfactant	Small mesopores Large mesopores	[86]
BiOBr	Triblock copolymer Pluronic (F127) L-Lysine Polyvinylpyrrolidone (PVP) CTAB	Nonionic surfactant Zwitterionic surfactant Nonionic surfactant Cationic surfactant	Stacked layers Flower-like hierarchical Block Sheet	[200]
TiO_2	CTAB SDS TritonX100 (TX100)	Cationic surfactant Anionic surfactant Nonionic surfactant	87% anatase phaseand, 52 nm 87% anatase phaseand 50% anatase phaseand, 97 nm	[201]
CdSe-graphene	CTAB Sodium lauryl sulfate (SLS)	Cationic surfactant Anionic surfactant	Good dispersion Clustered	[202]

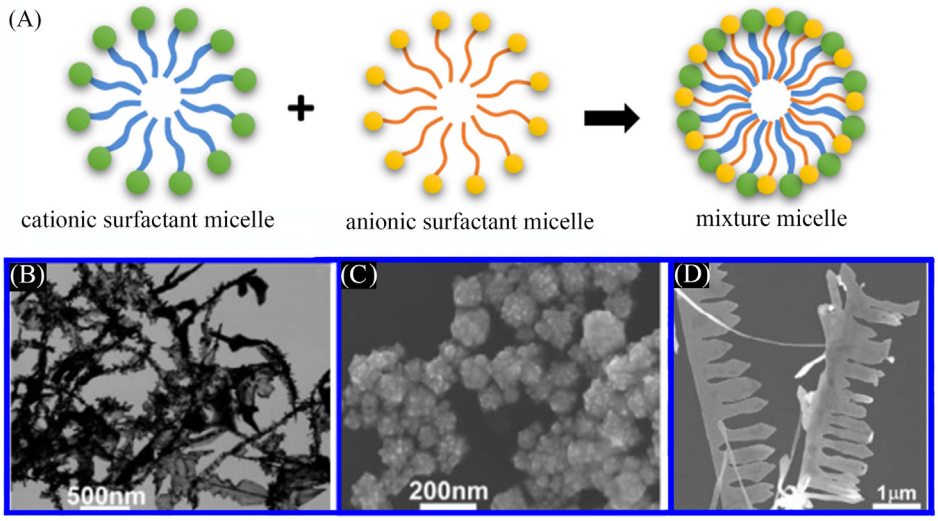

Fig. 6. (A) Mixed micelle formation from the oppositely charged surfactants. SEM images of gold nanocombs obtained in aqueous solutions of (B) single surfactant CTAB, (C) SDSn and (D) double surfactants. Reproduced with permission from Ref. [85]. Copyright 2008 American Chemical Society.

SDS mixed surfactant on the (2 1 1) surface at 4 °C and the (1 1 0) surface at 27 °C was weak, resulting in the formation of (1 1 0) and (2 1 1) oriented nanobelts at 4 and 27 °C, respectively [85]. Therefore, the lateral growth of the crystal was restricted in this way, resulting in long and thin photocatalysts formation.

3.1.2. The shape of surfactant

The shape of surfactants affects the structure and morphology of the crystal, such as the size and steric hindrance of the surfactant. On the one hand, the pore size of the crystal is related to the size of the surfactant, namely, the small size of the surfactant facilitates the formation of small pore size nanoparticles. CTAB and PEG were employed as the surfactants to synthesize the loaded TiO_2 on such silica-clay composite [86]. According to the different sizes of the surfactants, two different pore size composites were finally obtained. The smaller mesopores composite (< 4 nm) was corresponding to CTAB and the larger mesopores composite (16–25 nm) was generated by PEG. On the other hand, it should be noted that steric hindrance is a key factor when the type of surfactants are similar. Zn_2SiO_4 nanoparticles have been successfully prepared by a sonochemical method, using anionic (SDS), cationic (CTAB), and polymeric (PVP and PEG) as surfactants, respectively [87]. As shown in Fig. 7A, the particle size of Zn_2SiO_4 synthesized by PVP-25000 was smaller than that by PEG-6000, which might be related to the high steric hindrance of PVP-25000. The strong steric hindrance

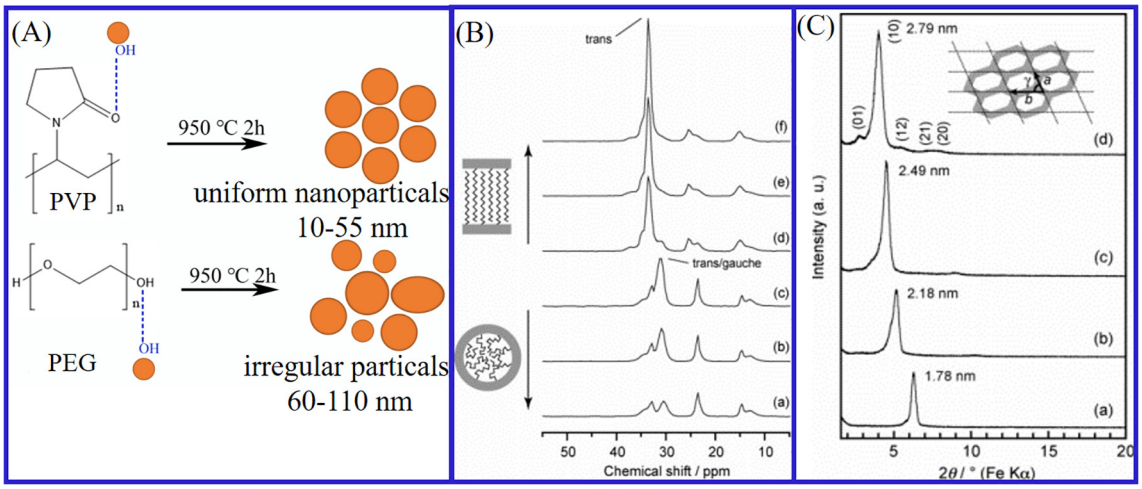

Fig. 7. (A) Schematic diagram of the effect of PVP and PEG on the size, morphology, and uniformity of products. Reproduced with permission from Ref. [87]. Copyright 2016 Elsevier. (B) ^{13}C CP/MAS NMR spectra and (C) XRD patterns of the derived from 1-(Cn). Reproduced with permission from Ref. [89]. Copyright 2005 American Chemical Society.

effect of surfactants prevented the growth of crystal particles, which resulted in the creation of small nanoparticles [71,87].

3.1.3. The length of the hydrophobic group of surfactant

Surfactants mostly are amphiphiles with hydrophilic and hydrophobic groups. The hydrophilic groups primarily contain heteroatomic functional groups, and the hydrophobic groups are often composed of hydrocarbon chains [73]. The hydrophilic groups can present charges on the surface of the nanostructure which minimize aggregation of the nanoparticles due to the repulsive charge. The water affinity of the surfactant end groups has attracted widespread attention, which determines the type, size and other characteristics of the aggregates [53]. Simultaneously, due to the van der Waals interaction between neighboring chains, the hydrophobic chains can interact with the surface of the nanoparticles to compact monolayers or bilayers [88]. The effect of different alkyl chain lengths (Cn, n is the number of alkyl chains) on the morphology of photocatalyst was studied in the self-assembly of oligosiloxane surfactant and alkyl chain into silica-based mesoporous structure. As shown in Fig. 7B, the peak intensity at 33.7 ppm gradually increased with the number of alkyl chains increased, which indicated that the number of trans chains and the order of the interlayer chains of the layered hybrids increased. However, the two-dimensional hexagonal structure was formed by the short alkyl chain of 6–10 (n). This might be due to the reduced effective hydrophobic volume of the short alkyl chain and the interdigitated arrangements of the long alkyl chains compensate for the intermolecular space resulted from the large headgroup [89]. Moreover, the long alkyl chains formed strong hydrogen bond interactions with each other, resulting in the formation of a compact bilayer structure [36]. The compact double layer caused the penetration of nascent atoms to be almost impossible to laterally nucleate. Therefore, these limited the lateral growth of the crystal and changed the growth direction of the crystal (Fig. 7C). As a result, the length of the nanorods clearly depended on the surfactant alkyl chain length.

3.1.4. The functional group of surfactant

In addition, the functional groups of surfactants are also important factors affecting the morphology of crystals. Functional groups, such as amino groups, can form strong coordination with positive ions in the crystal by forming interaction forces with the crystals, which changes the combined approach of crystal complexes [73,90]. Some of the groups in the surfactant can form hydrogen bonds with the hydroxyl groups on the surface of the crystal. For example, the presence of the PVP was very favorable to producing well-structured Zn_2SiO_4 nanoparticles. This was attributed to the fact that the oxygen atom in the carbonyl groups of PVP could form hydrogen bonds with hydroxy groups of Zn_2SiO_4 surface. As a result, the surfactant could be tightly wound around the surface of the crystal [87]. In addition, in the dual surfactant system, the introduction of groups in the surfactant also affects the formation of crystals. The addition of benzyldimethylhexadecylammonium chloride (BDAC) given long and thin photocatalyst in the presence of only CTAB in the preparation of gold nanorods [91]. At the same time, it was accompanied by a decrease in the aspect ratio and an increase in the diameter of the rod. That might be due to the fact that the presence of a benzyl ring caused additional non-polarities, resulting in a mixed surfactant having a smaller micelle size than that of CTAB micelle.

3.2. The effect of surfactant concentration

Surfactant concentration is an important factor affecting the structure and properties of the photocatalyst prepared by the surfactant [92], which mainly affects the density and viscosity of the solution [36], the capping effect of the surfactant on the crystal plane [93], crystal self-assembly [56] and crystal growth direction [73].

Firstly, surfactant concentration affects the orderly crystal growth during crystal formation by affecting the density and viscosity of the solution. In the low density and viscosity environment, the diffusion resistance is small, which is conducive to the ordered growth of nanowires and nanoribbons with high aspect ratios [36]. Ag/AgCl/GO quasi-nanocubes were synthesized in an oil-in-water medium by using CTAC as a surfactant [94]. As shown in Fig. 8A, the shape of the composite could be controlled by adjusting the concentration of CTAC. It was advantageous to form spherical particles at low concentrations and cubic particles at high concentrations.

In addition, it has been found that the crystals obtained are more uniform and dispersion in the high concentration of surfactant than that of low concentration [44,95,96]. The α-Fe_2O_3 with narrow size was developed by using different amounts of PVP surfactant [93]. As shown in Fig. 8B, with the concentration of PVP increased, the α-Fe_2O_3 with uniform size and good dispersion was obtained. This might be attributed to the surfactant being adsorbed on a specific crystal plane of the crystal, which is called as capping effect. When the concentration of PVP was very low, the capping effect was insufficient to cover or passivate crystals, resulting in the aggregation of crystal particles. If the PVP concentration was suitable, electrostatic repulsive or steric barrier interaction would prevent the aggregation of crystal particles. In the case of a thin film photocatalyst, increasing the surfactant

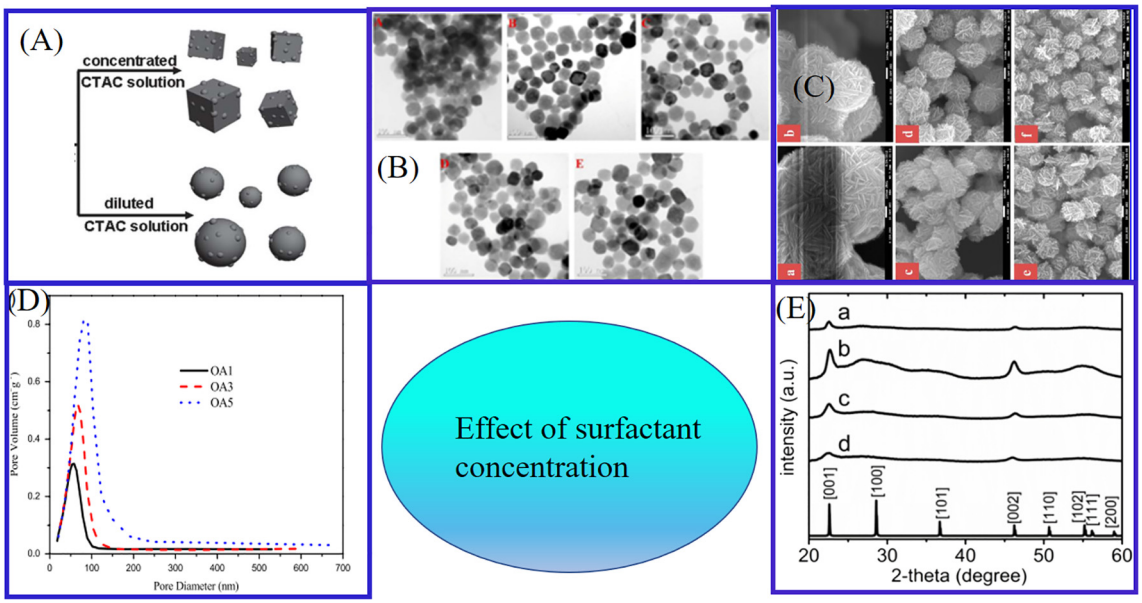

Fig. 8. The effect of surfactant concentration on (A) shape structure. Reproduced with permission from Ref. [94]. Copyright 2011 Royal Society of Chemistry. (B) Dispersibility. Reproduced with permission from Ref. [93]. Copyright 2012 American Chemical Society (C) particle size. Reproduced with permission from Ref. [101]. Copyright 2013 American Chemical Society. (D) Pore size distribution. Reproduced with permission from Ref. [104]. Copyright 2012 IOPscience (E) crystal growth direction. Reproduced with permission from Ref. [73]. Copyright 2011 Royal Society of Chemistry.

concentration causes an increase in the viscosity of the surfactant solution, which leads to an increase in film thickness [95,97].

In general, as the concentration increases, the particle size of the crystal decreases [98,99]. In the study of synthetic TiO_2, CTAB molecules were used as surfactant, and the effect of surfactant concentration on crystals was investigated [100]. As the amount of CTAB increased from 55 to 137 mM, the particle diameter of TiO_2 progressively decreased from 240 to 156 nm (Fig. 8C) [101]. Nevertheless, it is not conducive to the production of crystal particles with small size when the concentration is too high. As the concentration of the surfactant increases, the critical micelle concentration (CMC) is reached, at which point the interfacial tension is minimal. The CMC of the surfactant also affects the structure of the crystal, and it is advantageous for the formation of small pore photocatalysts for surfactants with a low CMC [102]. Fluorinated surfactants are special surfactants with a low CMC, which gives crystals with a small pore size [103]. The surfactant forms micelle that promotes self-assembly of the crystal when the concentration exceeds CMC [30,56]. In addition, the surfactant concentration also has an effect on the pore size of the crystal. According to the BJH pore size distribution of the carbon-doped TiO_2 nanoparticles, it exhibited a significant shift toward large pore diameter with the concentration of the surfactant oleic acid (OA) increased (Fig. 8D). This might be mainly due to the OA as a pore-structure-forming agent, which could increase pore coagulation especially at high concentrations leading to high porosity and large pores [104].

In addition to the morphology and size of the crystal, the concentration of the surfactant also affects the growth direction of the crystal [105,106]. In order to understand the influence of surfactant SDS on the growth of the Nb_2O_5 nanorods, the XRD spectra of Nb_2O_5 prepared by different concentrations of SDS were studied [73]. As shown in Fig. 8E, with the increase of SDS concentration, the intensity of the diffraction peak of the Nb_2O_5 at (1 1 0) planes initially increased and then decreased. This may be attributed to the high concentration of SDS hindering the growth of the nanorods in the (0 0 1) direction, resulting in a nonuniform and agglomerated product. In addition, the change in the crystal growth direction of crystals is often accompanied by the occurrence of lattice defects. The ZnO nanorods gradually grew in the radial direction with the SDS concentration increasing, which lead to the formation of dense lattice defects. The photocatalytic activity was improved due to the good crystallinity and the interstitial nanospaces of the radial rod [107].

3.3. The effect of solution pH

The pH value of the precursor solution is another important factor affecting the structure and shape of the final crystal. There are many differences in crystal morphology and structure between acidic and alkaline solution environments [42,108,109]. In order to study the restricted non-covalent interaction of ZnTPP in CTAB surfactant micelles, a series of nanocrystals with different morphologies were synthesized. The size of the crystal increased with the pH. In addition, the shape of the particles gradually became apparent as the concentration of the surfactant increased under different pH conditions [56]. For the other group of porphyrin crystals, the crystal shape changed from a cubic structure to a rod-like structure when the pH was changed from 11.5 to 2.0 [110].

A directed aggregation mechanism has been proposed to explain the formation of specific morphological crystals [111]. In this mechanism, the primary particles preferentially self-assemble into highly ordered superstructures, which have a clear external morphology. As shown in Fig. 9A, surfactant polyethylene oxide-polypropylene oxide-polyethylene oxide (P123) molecules were adsorbed on the surfaces of the primary $BiVO_4$ nanoparticles at a low pH value (pH < 3.0) [42]. The surfactant adsorbed on the surface of the crystal formed primary particles. Primary particles preferentially self-assembled into highly ordered superstructures, which hindered the further growth of the crystal. Due to the interaction of nanoparticles, a porous monoclinic $BiVO_4$ microscopic object with an olive-like morphology was obtained. When the pH was adjusted to 7.0, vanadium and niobium were presented in the form of VO_3^- and $BiONO_3$, respectively. They further reacted to form a $BiVO_4$ crystal nucleus. These nanoparticles eventually self-assembled into short rod-shaped $BiVO_4$ nanoparticles after the surfactant was removed by calcination. As the pH further increased to 11.0, primary $BiVO_4$ nanoparticles could not be formed due to the strong complexing ability between Bi^{3+} and OH^- ions in the precursor solution. The dodecylamine molecule could undergo a complex reaction with the formed complex, then assembling into a sheet-like entity. Finally, porous sheet-like spherical $Bi_4V_2O_{11}$ particles were formed after

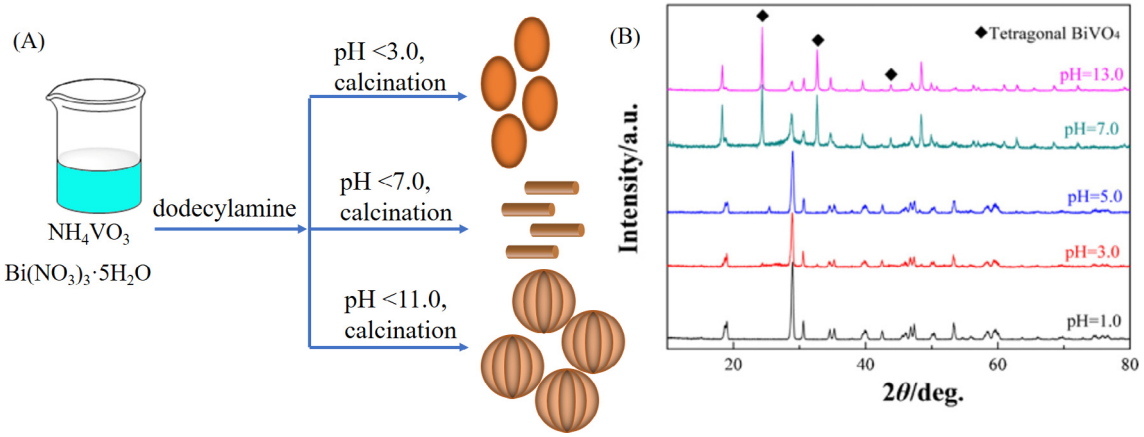

Fig. 9. (A) The $BiVO_4$ particles with various morphologies synthesized under different pH value conditions. (B) The XRD patterns of $BiVO_4$ synthesized under different pH value conditions. Reproduced with permission from Ref. [61]. Copyright 2013 Elsevier.

aggregation and crystallization. In addition, the pH of solution also affects the crystal structure type, which often leads to a change in crystal type [112]. The XRD patterns of the $BiVO_4$ samples are shown in Fig. 9B, from which it could be seen that $BiVO_4$ showed a monoclinic scheelite type at low pH. However, when the pH of the current bulk solution was high, the $BiVO_4$ sample showed a tetragonal structure type (t-$BiVO_4$) [61].

Apart from affecting the morphology and type of crystals, the pH value of precursor solution sometimes also affects the composition of the final product [42]. The Zn_2GeO_4 nanorods were prepared by the hydrothermal method using CTAB as a surfactant, and the effect of pH on the samples was studied [113]. The results showed that the composition of the product was closely related to the pH value. When the pH of the precursor solution was 5–6, the sample consisted of H_2GeO_3. However, a mixed sample $Zn(OH)_2$ and Zn_2GeO_4 was obtained at pH > 8, which was mainly related to the hydrolysis of substances. The precursor of GeO_2 was hydrolyzed to form $HGeO_3^-$. When the concentration of $HGeO_3^-$ and Zn^{2+} reached the supersaturation of Zn_2GeO_4, a small Zn_2GeO_4 core was formed. With the further grew of the nucleus, the Zn_2GeO_4 crystal was finally obtained. According to Eq. (3), increasing of the solution pH would reduce the concentration of Zn^{2+} and generate more $Zn(OH)_2$. In contrast, under acidic conditions, a high concentration of Zn^{2+} could be generated, which encouraged the generation of more Zn_2GeO_4 according to Eq. (2). In addition, the unreacted $HGeO_3^-$ could form H_2GeO_3.

$$GeO_2 + H_2O \rightarrow HGeO_3^- + H^+ \quad (1)$$

$$2Zn^{2+} + HGeO_3^- + 3OH^- \rightarrow Zn_2GeO_4 + 2H_2O \quad (2)$$

$$Zn^{2+} + 2H_2O \rightarrow Zn(OH)_2 + 2H^+ \quad (3)$$

3.4. The effect of synthesis method

As is known to all, the morphology and structure of the photocatalysts depend on synthesis method, which affects the microstructure and properties of the photocatalysts [114–116]. Many researchers have studied the effects of different preparation methods on photocatalyst properties [117,118]. Tian et al. prepared TiO_2/MWCNTs by sol-gel method and solvothermal method with benzyl alcohol as a surfactant, named SG-MWCNTs/TiO_2 and SG-MWCNTs/TiO_2, respectively, and they also studied the effects of two preparation methods on the photocatalysts [115]. According to the XRD spectrum, it could be concluded that the peak intensity of SG-MWCNTs/TiO_2 (20%) was weak, which indicated that the TiO_2 nanoparticles prepared by the sol-gel method was small and they had a low crystallinity. It could be seen from the TEM spectrum that TiO_2 nanoparticles aggregated on the surface of the CNT in the sol-gel system. However, dispersion of CNTs and nucleation of TiO_2 on the surface of CNTs might be promoted due to high pressure and high temperature environments in a solvothermal reaction. Therefore, the TiO_2 nanoparticles were uniformly decorated on the CNTs. The results of catalytic degradation experiments showed that ST-MWCNT/TiO_2 (20%) had higher photocatalytic activity than SG-MWCNT/TiO_2 (20%).

3.5. The effect of calcination temperature

In general, there are usually some residual substances on the surface of crystal after surfactant self-assembly, such as surfactants and solvents. The presence of these substances on the crystal faces affects the charge transfer, electromagnetic field strength and catalytic activity of the final photocatalyst [43,119]. Therefore, in order to increase the photocatalytic efficiency of the photocatalyst, it is necessary to remove the surfactant remaining on the surface of the crystal.

In most cases, calcination is an effective method for removing organic surfactants remaining on the surface of the crystal. In addition, calcination can improve the crystallinity of the photocatalyst, control the crystal transformation and improve the photocatalytic activity [120]. Moreover, according to the results of many literatures, different calcination temperatures also affect the catalytic activity of surfactant-assisted synthesis of photocatalyst [87,121]. Nanostructured $ZnIn_2S_4$ were formed by using oleylamine as the surfactant, and the effect of calcination temperature on crystal morphology was studied [122]. Three peaks (0 0 6), (1 0 2), and (1 1 0) were observed in the XRPD of the product prepared at 200 °C. When the calcination temperature had risen to 300 °C, these peaks became sharper and more pronounced than that of 200 °C. At the same time, the peak intensities at (1 0 1), (1 0 2), and (1 1 0) increased, which indicated the increase of crystallinity. In addition, the change of the calcination temperature also resulted in the transformation of the crystal type. In the synthesis of bimodal porous TiO_2 by using benzyl alcohol as a surfactant, the structures of the calcined TiO_2 samples at different temperatures were characterized by XRD [123]. As the temperature increased to 500 °C, the intensity of the anatase-TiO_2 diffraction peak became strong and sharp. However, when the calcination temperature was raised to 650 °C, the intensity of the diffraction peak decreased, and a rutile-type TiO_2 derivative appeared. The samples were all rutile at this time. These indicated that heat treatment caused the growth of crystal size and subsequent phase transitions at 800 °C. Therefore, the calcination temperature affects the catalytic activity of the photocatalyst by regulating the morphology and crystalline form of the photocatalyst [83].

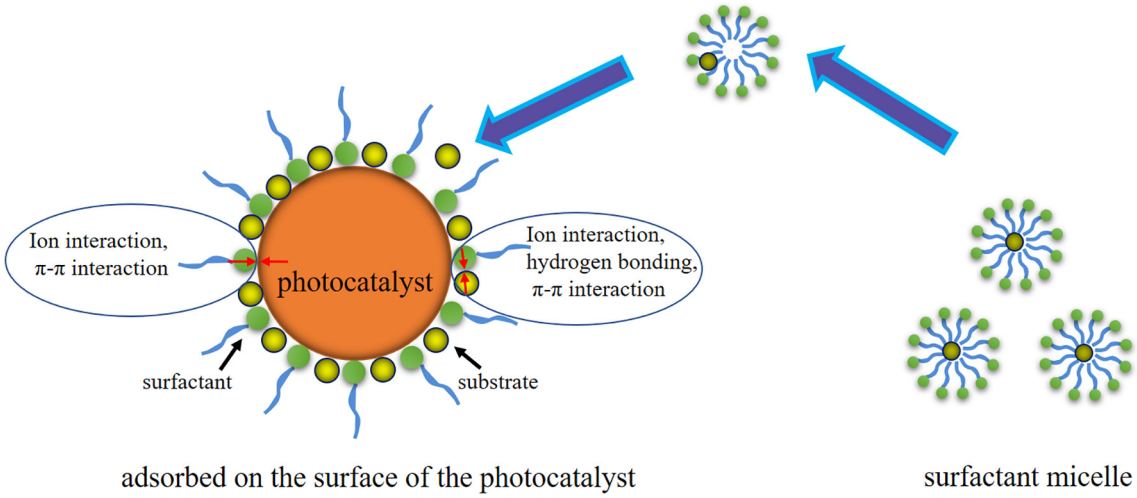

Fig. 10. The possible mechanism of the enhanced adsorption of substrate onto photocatalyst surface in the presence of surfactants.

3.6. The effect of direct addition of surfactants in degradation solution

In addition to improving the catalytic efficiency by modifying the photocatalysts during the preparation process, the surfactant can also be directly added to the degradation liquid to improve the degradation efficiency of the photocatalyst, and the possible mechanism is shown in Fig. 10. On the one hand, many surfactants and photocatalysts can form ionic interactions or π-π interactions, which is beneficial to enhance the dispersion of the photocatalyst in the solution and reduce aggregation. On the other hand, the adsorption of surfactant molecules on the surface of the photocatalyst particles must be specially considered. The surfactant forms a single layer or double layer adsorption on the surface of the photocatalyst by ion-dipole interaction or hydrogen bonding. The adsorbed surfactant is capable of partitioning the substrate molecules and reduce surface energy, which increases the density of active central atoms exposed on the surface, thereby facilitating photocatalytic activity [48]. Therefore, the substrate molecules have more opportunities to occupy the active sites on the surface of the semiconductor [124–126]. In the process of degradation of norfloxacin (NOF) by Bi_2WO_6, the introduction of nonionic TX100 significantly improved the degradation efficiency [127]. The TX100 molecule could easily bind to the surface of Bi_2WO_6 through a hydrophilic group such as a hydroxyl group. The surface-bound TX100 could pull the substrate molecule NOF close to photocatalyst surface through hydrophobic interactions. In addition, the electron transfer between the semiconductor surface and NOF was promoted by the π-π interaction. Therefore, the addition of surfactant TX100 improved the photocatalytic degradation efficiency of Bi_2WO_6 to NOF.

In addition, partially amphiphilic surfactants can increase the solubility of the substrate molecules in aqueous solution, thereby significantly enhancing the adsorption of substrate molecules on the surface of the photocatalyst particles and promoting the degradation rate of the contaminants [128,129]. Some pollutants, such as toluene, naphthalene, have low solubility in water and often float on the surface of the water. In order to enhance the contact of the contaminant with the photocatalyst, the use of a surfactant to reduce the surface tension helps to overcome the rate-limiting step and improve the solubility of the contaminants. Therefore, the addition of the surfactant increases the chance of contact between the substrate molecules and the photocatalyst, which is advantageous for improving the catalytic degradation efficiency. Zhang et al. studied the effect of surfactant TX100 micelles on photocatalytic degradation of phenanthrene by TiO_2 [129]. On the one hand, the amphiphilic structure of TX100 can increase the solubility of phenanthrene in water, which significantly enhances the adsorption of phenanthrene on the surface of TiO_2 and increases the degradation rate of photocatalyst to pollutants. On the other hand, the authors also studied the effect of the concentration of TX100 on the degradation of phenanthrene by TiO_2. TX100 micelles provide a hydrophobic center that increases the degradation rate of phenanthrene at a low concentration. However, the photocatalytic degradation rate of phenanthrene is reduced when the concentration of TX100 is more than 2 g/L. This is attributed to the excess micelles hinder the movement of the micelles containing phenanthrene, thereby reducing the adsorption of phenanthrene by titanium dioxide.

4. Recent advances of surfactant-assisted synthesis of photocatalysts

Based on a large number of researches, the surfactant-assisted synthesis of photocatalysts has been greatly developed. As shown in Fig. 11, current researches are primarily concerned with adding of other substances during the synthesis process, combing with other modification techniques (eg, doping element, building composites), using theoretical calculations to analyze mechanism and developing new surfactants.

4.1. Adding of other substances

Some literatures have studied the effects of the addition of substances, such as ionic liquids, organic additives or coordination chemistry, on crystal formation [61,130,131]. They can act as pore structure templates, reducing agents and reaction rate control agent.

The principle of orderly graded porous mesocrystalline liquid crystal phase can be produced based on the self-assembly of surfactant and oppositely charged polyelectrolytes [31]. Firstly, anionic polymer PAA was added to the cationic surfactant CTAB, and then self-assembled into a composite complex colloid by electrostatic interaction as a structure directing agent. The negatively charged phosphonic acid molecules were then uniformly incorporated into the composite colloid by electrostatic interaction. Secondly, hydrolysis and polymerization began to occur after the active $TiCl_4$ substance was added. During this process, some of the PAA chains were separated from the complex to form a PAA chain domain that could serve as a template for internal pore formation. Finally, a graded mesoporous titanate-based metal organic skeleton photocatalyst HM-TiPPh was obtained, as shown in Fig. 12A–D. Photocatalytic experiments showed that HM-TiPPh had good photocatalytic hydrogen evolution rate and stability.

In addition, it has been reported that the third component is added as a reducing agent to control the composition, structure, and morphology of the photocatalyst [65]. Nguyen et al. used CTAB as a

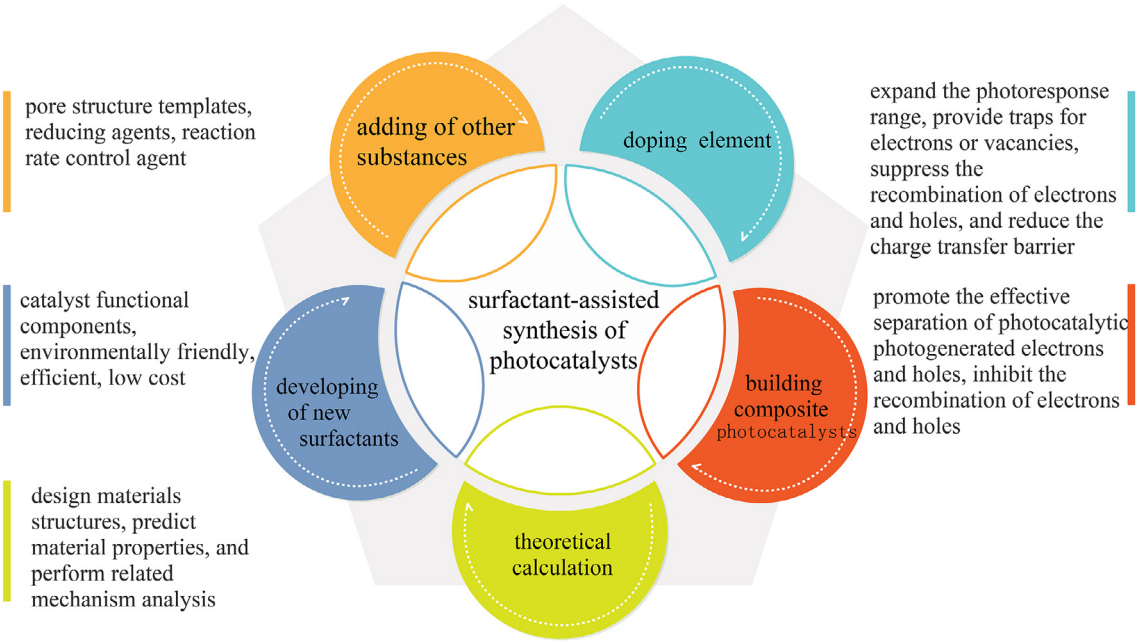

Fig. 11. Recent advances of surfactant-assisted synthesis of photocatalysts.

surfactant to prepare Cu_2O photocatalyst and studied the effect of glucose as a reducing agent on the reaction [38]. The amount of glucose in the reducing agent affected the composition, size, and shape of the photocatalyst. As shown in Fig. 12E–H, the particle size of Cu_2O increases with Cu^{2+}: glucose ratio. Besides, the prepared sample contained a large amount of CuO when the glucose concentration was not higher than the Cu^{2+} concentration. The rate of reduction could be controlled due to the isomerization of glucose. Therefore, glucose as a reducing agent can effectively control the composition, morphology, and size of the photocatalyst.

However, the synthetic reaction rates of some photocatalysts are too fast. In order to obtain a well-structured photocatalyst, it is necessary to control the reaction rate. Research in this area has been reported in the scientific literature. In the preparation of TiO_2, the alkoxide titanium precursor hydrolyzed rapidly and then condensed to form a Ti–O–Ti network structure [132]. Unfortunately, this rapid reaction caused the amorphous particles to precipitate rapidly and their structure was uncontrolled. Choi et al. prepared a controlled TiO_2 film by sol-gel method and Tween 80 surfactant as pore director [133]. Acetic acid (AcOH) was used as the titanium dioxide sol modifier in an ethanol solvent. The results showed that the successful synthesis route of Ti–O–Ti inorganic network had controllability. The reaction process is as follows:

$$iPrOH + AcOH \rightarrow iPrOAc + HOH \quad (4)$$

$$Ti - OiPr + AcOH \rightarrow Ti - OAc + iPrOH \quad (5)$$

$$Ti - OAc + iPrOH \rightarrow iPrOAc + Ti - OH \quad (6)$$

$$Ti - OiPr + Ti - OAc \rightarrow iPrOAc + Ti - O - Ti \quad (7)$$

In this case, the titanium-bonded acetate ligand could participate in hydrolysis and polymerization to finally obtain Ti–O–Ti. This mechanism indicates that the addition of AcOH reduces the hydrolysis and polymerization rate of the precursor and acts as a controllable agent for the crystal.

4.2. Doping element

As shown in Table 3, with the development of surfactant-assisted synthesis of photocatalysts, the research on its combination with other

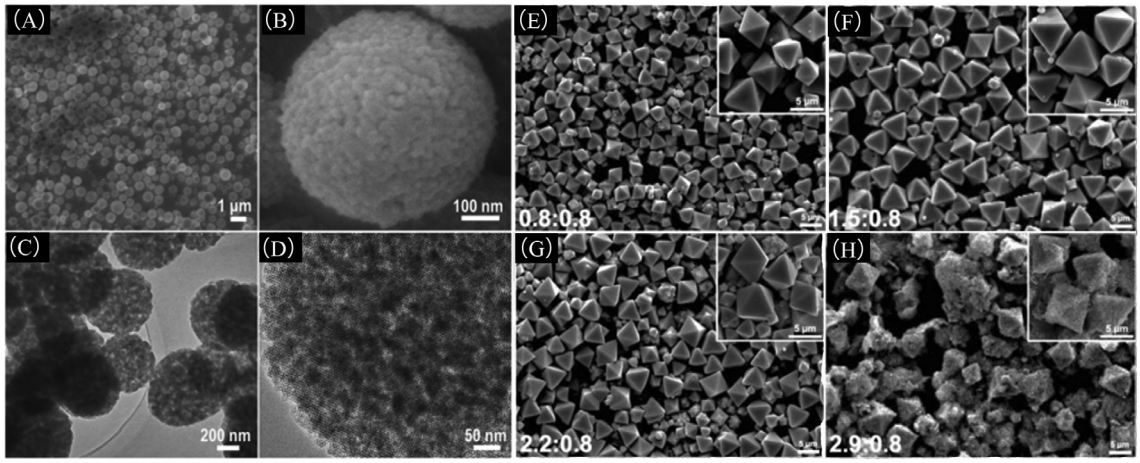

Fig. 12. (A, B) SEM and (C, D) TEM images of HM-TiPPh. Reproduced with permission from Ref. [31]. Copyright 2018 Wiley. SEM images of the Cu_2O synthesized at Cu^{2+}: glucose mole ratios of (E) 0.8:0.8, (F) 1.5:0.8, (G) 2.2:0.8, and (H) 2.9:0.8. Reproduced with permission from Ref. [38]. Copyright 2015 American Chemical Society.

Table 3
The combination of surfactants and other photocatalyst modification technologies in photocatalyst synthesis.

Modification techniques	Surfactant	Photocatalyst	Ref.
Doping element	Cetyltrimethylammonium bromide (CTAB)	N-doped $Bi_2O_2CO_3$	[43]
	Tetrabutylammonium chloride, tetrabutylammonium bromide, tetrabutylammonium iodide	BiOXs	[138]
	Polyethylene oxide-polypropylene oxide-polyethylene oxide (P123)	P-doped TiO_2	[203]
	Tween 80	S-doped TiO_2	[134]
	P123	Ag/V codoped TiO_2	[79]
Building composite photocatalysts	CTAB, sodium lauryl sulfate	SiO_2/CdSe-graphene	[202]
	CTAB	Bi_2WO_6-graphene	[204]
	Sodium dodecyl sulfate (SDS)	HT-DS/2TiO_2	[205]
	Glucose	TiO_2@Au@C	[141]
	Graphene oxide (GO)	Au-Pd/GR	[206]
	CTAB	BiOBr/montmorillonite	[207]
	Laurylamine hydrochloride	TiO_2–In_2O_3	[208]
	Triton-X100 (TX100)	CeO_2–TiO_2	[209]

photocatalysts modification technologies has become more frequent. Among the many modification technologies, doping element can expand the photoresponse range of the photocatalyst and provide traps for electrons or vacancies, suppress the recombination of electrons and holes, and reduce the charge transfer barrier [134–136].

The introduction of doping elements is derived from surfactant or other component in surfactant-assisted synthesis of photocatalyst [102,137]. Surfactants are generally non-metallic and partially contain N, P, and Cl, etc. These elements can be introduced into the photocatalyst by doping method [43,138]. On the one hand, the regulation of the surfactant can be exerted to regulate the growth of the crystal. On the other hand, doping by introducing elements improves the physicochemical properties of the photocatalyst. They work together to increase the photocatalytic reaction rate of the photocatalyst. Hyeok et al. used a sol-gel method to synthesize N-TiO_2 with high catalytic performance under visible light by using a nitrogen-containing surfactant DDAC as a nitrogen source [139]. On the one hand, DDAC was used as a pore template material to regulate the structure and properties of mesoporous TiO_2. On the other hand, DDAC was used as a nitrogen dopant to fill the band gap of TiO_2 to reduce its band gap. The method simultaneously realized the synthesis of mesoporous TiO_2 and the doping of nitrogen. By studying the physicochemical properties and electronic structure of TiO_2 before and after N doping, it was shown that the effective optical band gap (E_g^{eff}) decreased after N doping, which meant that N doping increased the visible light response of TiO_2 photocatalyst. At the same time, according to the X-ray photoelectron spectroscopy XPS characterization results, the electron density around the Ti atoms after doping was indicated. These changes in physicochemical properties and electronic structure indicated that the visible light catalytic performance of TiO_2 after N-doping was improved.

However, most surfactants are non-metallic surfactants, with the exception of some precious metal surfactants such as Iridium-, ruthenium-, rhodium-, and gadolinium-based metallosurfactants. To the best of our knowledge, it is lack of literature available to obtain doped photocatalysts by metallosurfactants. Therefore, the doping of some metal elements requires the introduction of other third components at present. Bouras et al. used Fe^{3+}, Cr^{3+}, and Co^{2+} as dopants, and TX100 as a surfactant to deposit a film of pure or doped titanium dioxide on a glass slide by using a sol-gel method [140]. The results showed that the presence of metal atoms resulted in changes in crystal size, partial loss of crystallinity, and transition from the anatase phase to the rutile phase. Moreover, the presence of Fe^{3+} led to a large redshift in the absorption wavelength of UV–Vis. This might be due to the excitation of electrons from ferric ions to the conduction band of the semiconductor. Conversely, the presence of Cr^{3+} ions in TiO_2 resulted in a structured spectrum, which was apparently due to the transition within the ions themselves. Co^{2+} doped TiO_2 produced a red shift in the visible spectrum and an additional broad absorption band at long wavelengths. Among the three cations, only Fe^{3+} doped TiO_2 nanocrystallites had photocatalytic behavior in the visible range. The efficiency increased to a maximum of 20% at high Fe^{3+} dopant concentrations.

4.3. Building composite photocatalysts

Aside from being applied to doped crystals, surfactants can also be used to control the formation of composite photocatalysts. The composite photocatalyst can promote the effective separation of photogenerated electrons and holes, and inhibit the recombination of electrons and holes. Therefore, the efficiency of the photocatalytic reaction is improved.

Hollow core-shell composites are ideal photocatalysts due to their low density, high specific surface area, low coefficient of thermal expansion and refractive index [141]. Wang et al. prepared monodisperse SiO_2-shell/ZnO-nuclear composite nanospheres in an oil-in-water microemulsion system [142]. The system used cyclohexane as the oil phase and TX100 as the surfactant. Finally, composite nanospheres with high core loading and adjustable shell thickness were obtained. In this study, the thickness of the SiO_2 coating affected the photocatalytic activity of ZnO nanoparticles. The thick SiO_2 shell resulted in low photocatalytic activity of the composite nanospheres. Under the thick SiO_2 shell, the composite nanosphere had high photocatalytic activity.

The carrier can serve to support and disperse the active component by supporting the metal oxide on the carrier, and at the same time, increase the strength of the photocatalyst [78]. Li et al. prepared CNT/TiO_2 nanoparticle with uniform-shell coating by a surfactant-coated sol-gel method from different TiO_2 precursors and sodium dodecyl benzene sulfonate (NaDDBS) surfactant-dispersed CNTs [143]. The photodegradation results of methylene blue had indicated that CNT/TiO_2 nanocomposites had high photocatalytic efficiency. Besides, the thickness of TiO_2 film was the key factor for controlling the electron transfer and photocatalytic activity of CNT/TiO_2 nanocomposites.

4.4. Using theoretical calculations

With the development of computing technology, theoretical calculations have been used to design photocatalysts structures, predict photocatalyst properties, and perform related mechanism analysis [144–147]. The surface energy is an important indicator when studying the effect of surfactants on crystals. Surface energy not only determines the surface structure and stability of the photocatalyst but also reflects the catalytic activity [57]. Su et al. used the calculation to study the effect of surfactant SDS on the surface of Cu_2O [48]. The surface termination and facet orientation of Cu_2O nanoparticles were precisely adjusted by adjusting the amount of hydroxylamine hydrochloride and surfactant. It was found that Cu_2O nanoparticles having a Cu-terminal (1 1 0) or (1 1 1) surface exhibited high photocatalytic activity. As shown in Fig. 13A–C, the results of density functional theory (DFT) simulations confirmed that SDS could reduce the surface free energy of

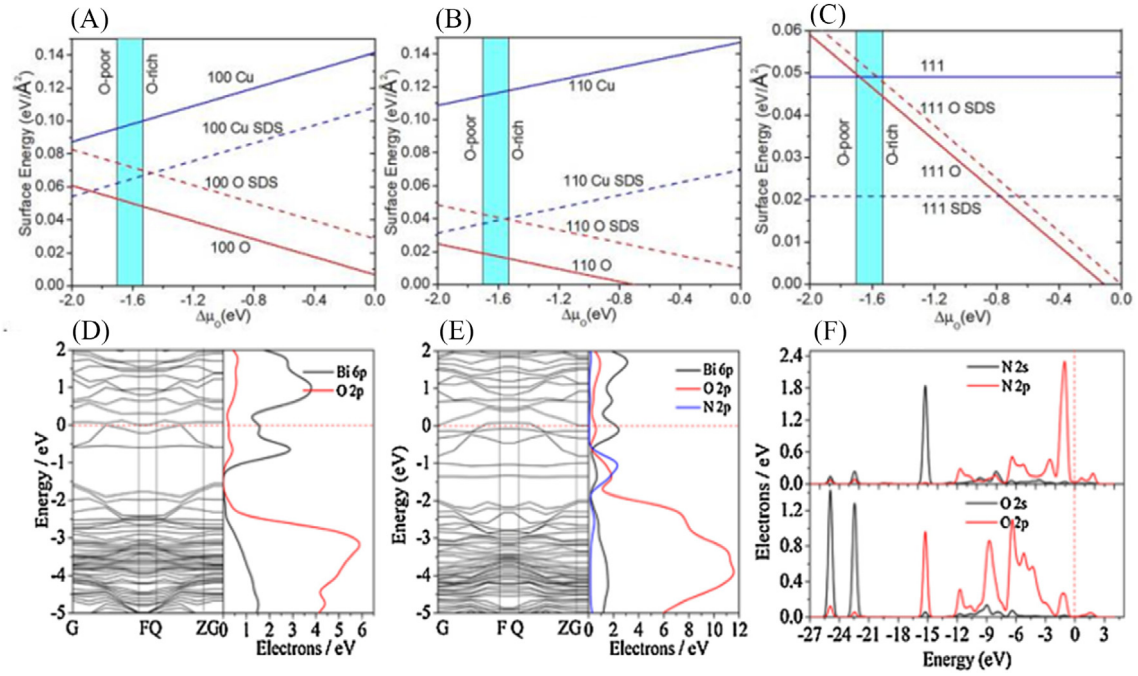

Fig. 13. Surface free energy of different Cu_2O surfaces: (A) (1 0 0), (B) (1 1 0) and (C) (1 1 1). Reproduced with permission from Ref. [48]. Copyright 2017 Elsevier. The band structure and DOS of (D) $Bi_2O_2CO_3$ (0 0 1) and (E) N-$Bi_2O_2CO_3$ (0 0 1) surface; (F) the partial DOS of N and O atoms in N-$Bi_2O_2CO_3$ (0 0 1) surface. Reproduced with permission from Ref. [43]. Copyright 2016 Elsevier.

Cu termination surface and increase the density of Cu atoms exposed on the crystal surface, which was beneficial to photocatalytic activity [148,149]. In addition, by studying the effect of SDS on the crystal morphology, the results showed that the SDS was chemically adsorbed by the SO_4CH_3 group. Therefore, the end face of Cu_2O was made to have high energy and a large amount of Cu exposed on the surface.

With the help of theoretical calculations, the elements of surfactant have been studied for the doping with crystals. Zhou et al. calculated the effect of the N doping of CTAB surfactant on the structural properties of $Bi_2O_2CO_3$ [43]. Through DFT calculation and XPS characterization, it was revealed that the N doping in the surface of $Bi_2O_2CO_3$ belongs to gap doping, and the formation of N–O bonds in the crystal lattice was revealed based on the change in the bond length of Bi–O. Furthermore, as shown in Fig. 13D and F, the hybridization between the N and O formed a dispersed valence band (VB) after nitrogen atoms were added, which facilitated the transfer of photogenerated carriers. Therefore, the surface N-doped $Bi_2O_2CO_3$ nanosheets exhibited strong visible light photocatalytic activity. Besides, it was confirmed that the electron density overlapping occurred between the N and O atoms after N doping, according to the partial density of states (DOS) as shown in Fig. 13F.

4.5. Developing new surfactants

Surfactants have unique surface chemistry, which has led to their application in many fields, and their demand will grow rapidly. However, in most existing self-assembly protocols, surfactants are used only as conditioning agents, which are subsequently removed by calcination rather than as a functional component to improve the catalytic activity of the photocatalyst. Therefore, the development of new surfactants for the construction of supramolecular nanoparticles remains a critical issue [150,151]. The edge of GO is mainly composed of a carbonyl group and a carboxyl group, and an epoxy group and a hydroxyl group are present on the surface of the substrate [152]. This gives GO an amphiphilic property, which is hydrophilic at the periphery and hydrophobic at the center. Therefore, GO can be used as a surfactant to regulate the synthesis of photocatalysts [68]. Guo et al. reported the formation of a 1D supramolecular zinc porphyrin (ZnTPyP) with a well-defined internal structure by self-assembly of a novel surfactant, namely GO [76]. Then, the photocatalytic degradation of rhodamine B was carried out by 1D ZnTPyP prepared by self-assembly of conventional surfactant CTAB and novel surfactant GO, respectively. The experimental results showed that ZnTPyP prepared by GO had higher photocatalytic degradation efficiency than photocatalyst prepared by CTAB.

Biosurfactants, such as various amino acids, have been widely used in the synthesis of nanostructures due to their good biocompatibility, water solubility and abundant functional groups in the molecular structure [153–155]. Cropek et al. used arginine as a surfactant to modify TiO_2 nanoparticles [153]. Compared with unmodified TiO_2, the arginine-modified TiO_2 photocatalyst completely changed the degradation pathway of nitrobenzene. During the degradation process, arginine could act as a hole trapping agent, thereby reducing electron/hole recombination and improving photocatalytic degradation efficiency. Dong et al. synthesized the Ce/Mo hierarchical structure by a simple method in the presence of surfactant amino acids [156]. Then, the photocatalytic activity of Ce/Mo photocatalysts for different dyes such as methylene blue, Congo red and methyl orange was studied. The experimental results showed that Ce/Mo had obvious photocatalytic degradation efficiency for Congo red under visible light irradiation.

5. The environmental application of surfactant-assisted synthesis of photocatalysts

The photocatalysts prepared by surfactants generally have a good morphology, active crystal face exposure, and excellent pore structure, resulting in excellent photocatalytic performance [31]. They are widely used in the environmental and energy fields due to their good catalytic performance [30,43,49]. As shown in Fig. 14, many researchers have reported the application of surfactant-assisted synthesis of photocatalysts in the environment, including pharmaceuticals, pesticides, organic dyes, benzenes, algal toxins, antibacterial, heavy metals, and toxic gases, etc., and relevant applications in recent years are summarized in Table 4.

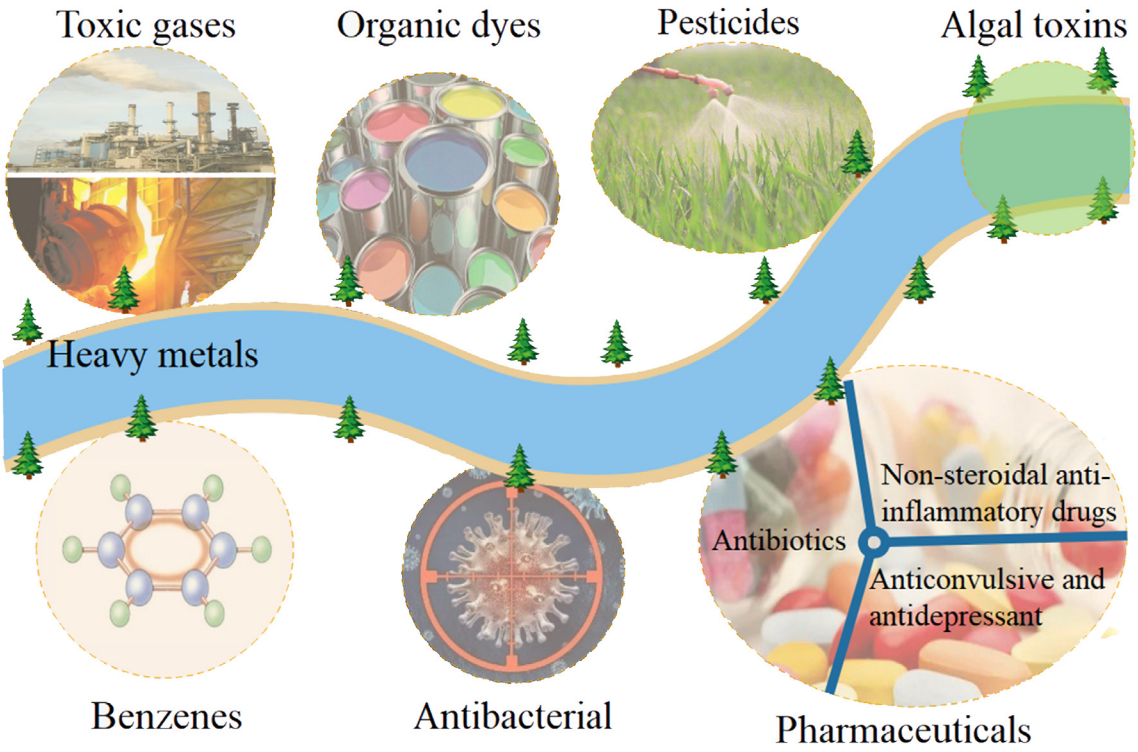

Fig. 14. Application in the environment of surfactant-assisted synthesis of photocatalysts.

5.1. Pharmaceuticals

With the development of the pharmaceutical industry and the increase in non-prescription drugs abuse, the problem of pharmaceuticals pollution has become increasingly serious, causing irreversible damage to the environment. Various pharmaceutical, such as antibiotics, anticonvulsants and antidepressants, and non-steroidal anti-inflammatory drugs, are often found in water. The use of photocatalyst technology to solve the problem of pharmaceuticals pollution has been reported by many people [157–159].

Table 4
Overview of researches on surfactant-assisted preparation of photocatalysts for enhanced pollutants removal.

Surfactant	Photocatalyst	Pollutant	Maximum removal rate	Ref.
Triton-X100 (TX100)	$Bi_4O_5Br_2$	Tetracycline hydrochloride	75%	[162]
Cetyltrimethylammonium bromide (CTAB)	SnO_2	Carbamazepine	97%	[7]
Polyethylene oxide-polypropylene oxide-polyethylene oxide (P123)	Sn-TiO_2	Ibuprofen	25%	[169]
n-Dodecylamine	Si-$CuF_{16}Pc$	2,4-Dichlorophenoxyacetic acid	90%	[210]
Polyvinylpyrrolidone (PVP)	H_2TPyP	Methyl orange	80%	[109]
PVP	BiOBr/Bi	Methyl orange	73%	[44]
Oleic acid (OA), oleylamine	$ZnIn_2S_4$	Methyl blue	66%	[122]
P123	$BiVO_4$	Methyl blue, phenol	90%	[149]
Sodium dodecyl sulfate (SDS)	Cu_2O	Methyl orange	90%	[48]
PVP	Zn_2SiO_4	Methyl orange	42%	[87]
Chiral liquid crystalline	CNLC–RGO–CLCS	Methyl blue	95%	[150]
sodium dodecyl sulfate (SDS)	BiOBr	Methyl orange	77%	[148]
SDS	Se	Methylene blue	90%	[71]
CTAB	Cu_2O	Methyl orange	90%	[38]
Myristyltrimethylammonium bromide	ZnTPP	Methyl orange	90%	[56]
$LiNO_3$	$PbTiO_3$	Methyl blue	99%	[211]
CTAB	BiOBr–Mt	Rhodamine B	99%	[207]
Alcohols	$SrTiO_3$	Methyl blue	76%	[151]
Sodium lauryl sulfate	CdSe-graphene	Methyl blue, reactive Black B	99%	[202]
P123	TiO_2	4-Chlorophenol	99%	[121]
TX100	Fe_2O_3	2-Chlorophenol, 2-nitrophenol	99%	[212]
Glucose	TiO_2@Au@C	4-Nitroaniline, 4-nitrophenol	93%	[141]
Triton X-114	$AgTiO_2$	4-Chlorophenol	90%	[174]
Dodecylamine	$BiVO_4$	Phenol	96%	[42]
Mesoporous silica	TiO_2	Nonylphenols, heptylphenol	99%	[213]
P123	Ag-AgBr/Al_2O_3	2-Chlorophenol, 2,4-dichlorophenol	99%	[214]
CTAB	$Li_9Fe_3(P_2O_7)_3(PO4)_2$	Phenol	70%	[81]
Tween 80	C-N-TiO_2	Microcystin-LR	70%	[181]
P123	C, N and S co-doped TiO_2	Microcystin-LR	100%	[215]
Cetyltrimethylammonium bromide (CETAB)	TiSi	Pb^{2+}, Cd^{2+}	100%	[189]
CTAB	N-doped $Bi_2O_2CO_3$	NO	30.4%	[43]

5.1.1. Antibiotics

Antibiotics are a class of chemicals that interfere with the developmental functions of other living cells. These pharmaceuticals are difficult to microbial degradation in environmental waters and are accompanied by environmental water migration and transformation. The photocatalytic degradation of antibiotics, such as tetracycline and sulfonamides, has received a lot of attention [160,161]. $Bi_4O_5Br_2$ with an adjustable 2D nanosheets was synthesized by using TX100 as a stabilizer and an ionized liquid-in-water microemulsion method [162]. The SEM and TEM results showed that the concentration of the surfactant significantly affects the morphology and size of the $Bi_4O_5Br_2$ crystal. The photocatalytic degradation of tetracycline hydrochloride showed that $Bi_4O_5Br_2$ has high photocatalytic efficiency under visible light irradiation, due to its hollow/layered spherical structure and Bi-rich strategies.

5.1.2. Anticonvulsive and antidepressant

Anticonvulsive pharmaceuticals, such as carbamazepine, buspirone, and amitriptyline, are persistent organic pollutants and difficult to biodegrade in environmental waters [163–165]. As a sedative, carbamazepine can cause serious toxicity in the hematopoietic and liver systems. In addition, it may reduce the ability of fish to escape [166]. However, carbamazepine is sensitive to photodegradation. Therefore, many studies have reported the photocatalytic degradation of carbamazepine by utilizing various photocatalysts [167]. Begum et al. conducted a photocatalytic degradation of carbamazepine by SnO_2 [7]. The SnO_2 nanoparticle size was controlled by the addition of a surfactant and adjusting the annealing temperature. The characterization results showed that the SnO_2 nanoparticles synthesized by the cationic surfactant CTAB (SC1) were smaller size than the SnO_2 nanoparticles synthesized with the anionic surfactant SDS (SS1). The average size of the SnO_2 nanoparticles formed at a lower annealing temperature of 300 °C was less than that synthesized at 600 °C. Degradation experiments showed that the degradation rates of carbamazepine in the synthesized SC1 and SS1 within 60 min was 97% and 92% under UV-C illumination, respectively.

5.1.3. Non-steroidal anti-inflammatory drugs

Non-steroidal anti-inflammatory drugs, such as diclofenac, ibuprofen, naproxen, and acetaminophen, are widely used as prescription and over-the-counter drugs because of their elasticity and stable chemical properties, which have been readily detected in environmental waters in recent years [168]. Compared with other pharmaceuticals, there are more studies on the photocatalytic degradation of these drugs. Solis-Casados et al. used a surfactant assisting technique with P123 as a template to obtain Sn-modified TiO_2 powders having different tin contents, which was advantageous for forming an anatase/rutile mixture at an annealing temperature as low as 350 °C [169]. Then, the photocatalytic degradation properties of TiO_2-based photocatalysts for NSAID, diclofenac, ibuprofen, and acetaminophen were investigated. The results indicated that each type of photocatalyst had selectivity or affinity for the degradation of a particular drug.

5.2. Pesticides

Pesticides, such as insecticides and herbicides, are developed to protect the growth of crops, but excessive pesticides can easily cause harm to people and the environment. For example, the pollution of soil, atmosphere, and groundwater by pesticides retained in the soil, which is one of the most toxic and dangerous chemicals to the water source [170]. Pesticide contamination is a global problem and there is an urgent need to apply efficient, economical and sustainable methods to solve it. Chlorpyrifos is a broad-spectrum organophosphorus pesticide, which is especially effective for the control of underground pests. It is used to pollute water when it is used for irrigation, which threatens human health. Perveen et al. synthesized the $Ti_{0.85}Sn_{0.15}O_2$ by the sol-gel method using the docusate sodium salt surfactant as a template [171]. The characterization results indicated that the surfactant played an important role in controlling the size and band gap of the photocatalyst, thus affecting the catalytic activity of the photocatalyst. Photocatalytic degradation of the chlorpyrifos showed that the pH value of the solution affected the photocatalytic degradation activity, indicating that the degradation reaction was related to ·OH and positive holes. At pH = 5.8, the maximum degradation rate was 92%.

5.3. Organic dyes

Organic dyes, such as methyl blue, methylene blue, methyl orange, methyl red and rhodamine B, etc., are mainly from the textile industry and cause serious pollution to river water, leading to changes in water ecosystems and serious threats to the lives of animals and plants [172,173]. Moreover, with the continuous development of the dye industry, dye wastewater has become a major source of water pollution. The surfactant-modified zinc silicate, zinc oxide and cerium oxide were reported for photodegradation of dyes in wastewater [44,87,150]. Zhou et al. prepared N doped BiOCl by using a nitrogen-containing CTAB surfactant [43]. The experimental results of photocatalytic degradation of RhB indicate that BiOCl-CTAB can completely degrade RhB in 10 min, while BiOCl takes 30 min. According to the UV–vis absorption spectrum, the band gap of BiOCl was decreased after the addition of CTAB. Consequently, CTAB-assisted synthesis of BiOCl has high photocatalytic activity.

There are many articles that report the removal of organic dyes using surfactant-assisted synthesis of photocatalysts. Zhu et al. synthesized Ag/AgBr/GO Nanocomposite via Oil/Water and Water/Oil Microemulsions [68]. The photocatalyst obtained when the GO was combined with Ag/AgBr has a small size, which is attributed to the unconventional polymeric surfactant GO acting as a blocking agent or stabilizer, hindering the growth of photocatalyst crystals. In addition, the effect of surfactant CTAB addition was also investigated. When CTAB is added, a direct microemulsion system is formed. In this oil/water microemulsion system, the polar head group ($–N(CH_3)_3^+$) and the counter ion (Br^-) of CTAB dissolve and induce the collision of Ag^+ and Br^- to produce AgBr, in which the reaction is mainly carried out on the outer surface of the oil phase. Therefore, the surface of AgBr is mainly blocked by Ag, resulting in relatively high photocatalytic activity. The results of photocatalytic degradation showed that the degradation rate of methyl orange by Ag/AgBr/GO prepared by oil/water microemulsion was 94%.

5.4. Benzenes

Benzenes, such as phenol, chlorophenol, and p-nitrophenol, are common pollutants emitted by human activities [174]. Many kinds of benzenes are toxic to organisms and can pose a direct hazard to human health. As a highly efficient photocatalyst, $BiVO_4$ has excellent physicochemical properties and crystal structure, which has received much attention in recent years [175,176]. A monoclinic $BiVO_4$ single crystal was obtained by a hydrothermal method using a triblock copolymer P123 as a surfactant [149]. The photocatalytic degradation efficiency of $BiVO_4$ to phenol under visible light irradiation was evaluated. The experimental results showed that after 4 h of visible light irradiation, the conversion of phenol was as high as 91% by $BiVO_4$, and the conversion rate of phenol was only 4% by commercial TiO_2 (P25). The efficient photocatalytic efficiency of $BiVO_4$ might be related to its high surface area, pore structure, low band gap energy, and particle morphology.

In addition to studying the photocatalytic degradation of phenol, it is also important to study the photocatalytic degradation behavior of phenolic derivatives. Mao et al. obtained different sizes of graded porous and (0 0 1) crystal face exposure ratios of Bi_3O_4Br by adjusting the concentration of surfactant TX100, and the photocatalytic degradation behavior of various phenol derivatives was studied [177].

The experimental results showed that the by the hollow spheres and the (0 0 1) crystal face exposed nanosheets assembled Bi_3O_4Br not only exhibited high-efficiency visible light photocatalytic performance for phenolic derivatives but also exhibited long-lasting and universal photocatalytic oxidation ability.

5.5. Algal toxins

In freshwater supplies, contamination of plant nutrients such as nitrogen and phosphorus can cause eutrophication of water bodies, causing some algae to grow wild, and these toxins threaten the public health of water supplies. Among most eutrophic waters, cyanobacteria are numerous and dominant species. Microcystin-LR is a kind of biologically active cyclic heptapeptide compound produced by many cyanobacteria commonly found in rivers [178,179]. It is the most widely distributed hepatic toxin and is listed in the new pollutant candidate list (CCL1-3) of the USEPA [180]. Therefore, there is an urgent need to develop an innovative and practical technology to solve this problem. Dionysiou, D. D research group has done a lot of research work to solve this problem. They had synthesized a series of TiO_2-based films photocatalysts with surfactants to study photocatalytic degradation of microcystin-LR [180–182]. C-N-TiO_2 films (5 layers) were prepared by the sol-gel method using nonionic surfactant tween 80 as pore director and carbon precursor [181]. The effects of different calcination temperatures on the structure and properties of the materials were investigated. The photocatalytic degradation of microcystin-LR showed that the photocatalyst prepared by surfactant and ethylenediamine could significantly improve the photocatalytic degradation activity compared with the photocatalyst prepared without them. This is attributed to the fact that the presence of carbon and nitrogen expands the light absorption range of the photocatalyst, effectively narrowing the band gap and inhibiting the transformation of anatase into rutile.

5.6. Antibacterial

Biological contaminants, such as bacteria, viruses, and fungi, can erode the hull and cause disease in humans, animals, and plants [183]. The photocatalyst can produce ·OH with the strong oxidizing property, which inactivated the bacteria's super-oxidation ability to destroy the cell membrane of the cell to cause bacterial death. In addition, it can also coagulate the virus protein and inhibit the virus activity to achieve the purpose of inactivating the virus [184,185]. Therefore, the photocatalyst has a strong bactericidal ability. Li et al. synthesized $ZnWO_4$ by hydrothermal method using three different surfactants, i.e. ((ethylene glycol) EG, (sodium dodecyl benzene sulfonate) SDBS, and CTAB) [186]. Then, the $ZnWO_4$ film was used as the anode to study the inactivation behavior of marine organisms under 2 V, 254 nm ultraviolet light. SEM and TEM results show that the surfactant can affect the morphology and microstructure of $ZnWO_4$. The results of degradation showed that all photocatalysts synthesized with the aid of surfactants showed enhanced activity compared to photocatalysts without surfactant synthesis. For example, the photocatalyst prepared with the EG surfactant has a microbial inactivation time of 7 min, while the photocatalyst prepared without a surfactant has a prolonged 36% for 11 min. This is mainly due to the fact that the EG sample prepared using the surfactant has a broadband gap and a high normal valence band, which is advantageous for the formation of holes having the strong oxidizing ability.

5.7. Other applications

In addition to the above applications in the environment, some literatures have reported the application of surfactant-assisted synthesis of photocatalysts in the catalytic transformation of heavy metal ions and toxic gases.

5.7.1. Heavy metals

Heavy metals can interact strongly with proteins and various enzymes in the human body, making them inactive and causing great harm to the human body [187,188]. In addition, heavy metals are highly enriched and difficult to degrade in the environment. Mishra et al. used CETAB as a surfactant to prepare a titanium dioxide photocatalyst mixed with silica and zirconia, respectively, and studied the removal of Pb^{2+} and Cd^{2+} in water [189]. The experimental results showed that the removal rate of the photocatalyst within 60 min is 89% in visible light. Moreover, the photocatalyst could achieve complete removal of Pb^{2+} and Cd^{2+} in 60 min by using sodium formate as an organic hole scavenger. After that, Mishra et al. synthesized spherical silica and zirconia mixed titanium dioxide through CTAB as a surfactant, and studied the effect of surfactant concentration and calcination temperature on the photocatalyst. The results of characterization and photocatalytic degradation experiments showed that the surfactant concentration had a great influence on the morphology of the photocatalyst and the calcination temperature affects the performance of photocatalyst degradation of lead.

5.7.2. Toxic gases

Toxic gases are mainly derived from industrial pollution, combustion of coal and oil, and spoilage of biological materials. It mainly includes ammonia, ozone, nitrogen dioxide, sulfur dioxide, carbon monoxide, hydrogen sulfide, etc [190,191]. It has a stimulating effect on the respiratory tract and is easily inhaled to cause poisoning. Zhou et al. prepared a N-doped $Bi_2O_2CO_3$ nanosheet photocatalyst by room temperature chemical method using a nitrogen-containing surfactant CTAB [43]. The results showed that the addition of CTAB not only affected the growth of crystallization but also changed the surface properties of $Bi_2O_2CO_3$ through the interaction between them. The formation of N–O bond improved the light absorption range and charge separation efficiency, which led to an increase in photocatalytic activity in visible light. At the indoor air levels, the photooxidation of NO by $Bi_2O_2CO_3$-CTAB could be as high as 30.4% in 5 min. Conversely, the photooxidation of NO by $Bi_2O_2CO_3$ is only 6.7% in 5 min.

Volatile organic compounds (VOCs) are a series of volatile organic compounds such as styrene, propylene glycol, glycol, phenol, toluene, and formaldehyde, etc., which threaten human life [192–194]. Wang et al. synthesized TiO_2 film by the sol-gel method, using Tween 80 as a surfactant [195]. Combined with SEM, it can be concluded that the prepared TiO_2 film has a large specific surface area, a uniform size and a compact structure, which was attributed to Tween 80 acts as a pore directing agent. In addition, photocatalytic degradation of formaldehyde by Al-supported TiO_2 film was also investigated. The experimental results show that the conversion rate of formaldehyde to TiO_2 thin film photocatalyst assisted by surfactant is 99%.

6. Conclusions and future prospects

Surfactants play an important role in the preparation of photocatalysts. This review summarizes the influencing factors in the surfactant-assisted synthesis of photocatalysts in detail. Firstly, the mechanism and synthesis method are reviewed, and then the affecting factors, including surfactant type, surfactant concentration, solution pH, synthesis method, and calcination temperature are discussed. The results showed that the reaction conditions affect the photocatalytic efficiency of the photocatalyst by regulating the morphology, composition, and crystal face exposure of the photocatalyst. Secondly, the recent advances of surfactant-assisted synthesis of photocatalysts are summarized. The recent advances, such as adding other substances during the synthesis process and combining with other photocatalytic modification techniques, using theoretical calculations and developing new surfactants are discussed in detail. Finally, the application of surfactant-assisted photocatalysts in the removal of pollutants from wastewater is summarized.

However, there are still some shortcomings in the surfactant-assisted synthesis of photocatalysts photocatalytic technology. For example, the mechanism of action of surfactants is still not clear, and the influencing factors in the synthesis of photocatalysts need further investigation. Therefore, in order to much more accurately use surfactants to adjust the formation of photocatalysts, further studies are still needed.

(1) Roles of surfactant. Although we have summarized the effects of surfactants in the preparation of photocatalysts, current research is not sufficient. Surfactants can act as shape control agents, dispersants, templating agents, and carrier, etc., which results in the complex mechanism of surfactants in the photocatalyst preparation process. Therefore, further research is needed.
(2) Influencing factor. In this paper, we mainly summarize the types of surfactants, indicating the effects of active agent concentration, solution pH, synthesis method and calcination temperature on surfactant-assisted photocatalysts. Further exploration is needed to explore the influencing factors, such as ultrasonic power, pressure, and mixing of the third component.
(3) Theoretical calculations. At present, the research on the surfactant-assisted synthesis of photocatalysts by theoretical calculations is rare, which is mainly focusing on surface energy. With the continuous development of theoretical calculations in the field of photocatalysis, the theoretical calculation can be used to achieve photocatalyst screening, design, structural property analysis (such as forbidden band, the density of states, electron density distribution), and mechanism analysis. However, the level of theoretical calculations has not been fully reflected in this field.
(4) Developing new surfactants. As people's awareness of environmental protection increases, it is imperative to develop new and environmentally friendly surfactants. At the same time, the use of biosurfactants in the preparation of photocatalysts should be expanded. In addition, new functional surfactants, such as graphite oxide, should also be developed.

Acknowledgments

The study was financially supported by the Program for Changjiang Scholars and Innovative Research Team in University (IRT-13R17), the National Natural Science Foundation of China (Nos. 51679085, 51579096, 51378192, 51039001, 51378190, 51521006, 51508177), the Fundamental Research Funds for the Central Universities of China (Nos. 531107050930, 531107051205), the Funds of Hunan Science and Technology Innovation Project (No. 2018RS3115), the Key Research and Development Project of Hunan Province of China (2017SK2241).

References

[1] X. Ren, G. Zeng, L. Tang, J. Wang, J. Wan, Y. Liu, J. Yu, H. Yi, S. Ye, R. Deng, Sorption, transport and biodegradation – an insight into bioavailability of persistent organic pollutants in soil, Sci. Total Environ. 610 (2018) 1154–1163.
[2] S. Ye, G. Zeng, H. Wu, C. Zhang, J. Dai, J. Liang, J. Yu, X. Ren, H. Yi, M. Cheng, C. Zhang, Biological technologies for the remediation of co-contaminated soil, Crit. Rev. Biotechnol. 37 (2017) 1062–1076.
[3] P. Xu, G.M. Zeng, D.L. Huang, C.L. Feng, S. Hu, M.H. Zhao, C. Lai, Z. Wei, C. Huang, G.X. Xie, Z.F. Liu, Use of iron oxide nanomaterials in wastewater treatment: a review, Sci. Total Environ. 424 (2012) 1–10.
[4] V.G. Samaras, A.S. Stasinakis, D. Mamais, N.S. Thomaidis, T.D. Lekkas, Fate of selected pharmaceuticals and synthetic endocrine disrupting compounds during wastewater treatment and sludge anaerobic digestion, J. Hazard. Mater. 244–245 (2013) 259–267.
[5] S. Gunti, A. Kumar, M.K. Ram, Nanostructured photocatalysis in the visible spectrum for the decontamination of air and water, Int. Mater. Rev. 63 (2018) 257–282.
[6] Z. Liu, Z. Zeng, G. Zeng, J. Li, H. Zhong, X. Yuan, Y. Liu, J. Zhang, M. Chen, Y. Liu, G. Xie, Influence of rhamnolipids and Triton X-100 on adsorption of phenol by Penicillium simplicissimum, Bioresour. Technol. 110 (2012) 468–473.
[7] S. Begum, M. Ahmaruzzaman, CTAB and SDS assisted facile fabrication of SnO_2 nanoparticles for effective degradation of carbamazepine from aqueous phase: a systematic and comparative study of their degradation performance, Water Res. 129 (2018) 470–485.
[8] Y. Zhou, X. Liu, L. Tang, F. Zhang, G. Zeng, X. Peng, L. Luo, Y. Deng, Y. Pang, J. Zhang, Insight into highly efficient co-removal of p-nitrophenol and lead by nitrogen-functionalized magnetic ordered mesoporous carbon: performance and modelling, J. Hazard. Mater. 333 (2017) 80–87.
[9] X.H. Lin, D. Sriramulu, S.F.Y. Li, Selective removal of photocatalytic non-degradable fluorosurfactants from reverse osmosis concentrate, Water Res. 68 (2015) 831–838.
[10] B. Shao, Z. Liu, G. Zeng, Y. Liu, X. Yang, C. Zhou, M. Chen, Y. Liu, Y. Jiang, M. Yan, Immobilization of laccase on hollow mesoporous carbon nanospheres: noteworthy immobilization, excellent stability and efficacious for antibiotic contaminants removal, J. Hazard. Mater. 362 (2019) 318–326.
[11] M. Cheng, C. Lai, Y. Liu, G. Zeng, D. Huang, C. Zhang, L. Qin, L. Hu, C. Zhou, W. Xiong, Metal-organic frameworks for highly efficient heterogeneous Fenton-like catalysis, Coord. Chem. Rev. 368 (2018) 80–92.
[12] Y. Liu, G. Zeng, H. Zhong, Z. Wang, Z. Liu, M. Cheng, G. Liu, X. Yang, S. Liu, Effect of rhamnolipid solubilization on hexadecane bioavailability: enhancement or reduction? J. Hazard. Mater. 322 (2017) 394–401.
[13] G.C. de Assis, E. Skovroinski, V.D. Leite, M.O. Rodrigues, A. Galembeck, M.C.F. Alves, J. Eastoe, R.J. de Oliveira, Conversion of “waste plastic” into photocatalytic nanofoams for environmental remediation, ACS Appl. Mater. Interfaces 10 (2018) 8077–8085.
[14] H. Yi, D. Huang, L. Qin, G. Zeng, C. Lai, M. Cheng, S. Ye, B. Song, X. Ren, X. Guo, Selective prepared carbon nanomaterials for advanced photocatalytic application in environmental pollutant treatment and hydrogen production, Appl. Catal. B: Environ. 239 (2018) 408–424.
[15] C. Zhou, C. Lai, C. Zhang, G. Zeng, D. Huang, M. Cheng, L. Hu, W. Xiong, M. Chen, J. Wang, Y. Yang, L. Jiang, Semiconductor/boron nitride composites: synthesis, properties, and photocatalysis applications, Appl. Catal. B: Environ. 238 (2018) 6–18.
[16] H. Shi, Y. Yu, Y. Zhang, X. Feng, X. Zhao, H. Tan, S.U. Khan, Y. Li, E. Wang, Polyoxometalate/TiO_2/Ag composite nanofibers with enhanced photocatalytic performance under visible light, Appl. Catal. B: Environ. 221 (2018) 280–289.
[17] H. Dong, G. Zeng, L. Tang, C. Fan, C. Zhang, X. He, Y. He, An overview on limitations of TiO_2-based particles for photocatalytic degradation of organic pollutants and the corresponding countermeasures, Water Res. 79 (2015) 128–146.
[18] J. Wang, L. Tang, G. Zeng, Y. Deng, Y. Liu, L. Wang, Y. Zhou, Z. Guo, J. Wang, C. Zhang, Atomic scale g-C_3N_4/Bi_2WO_6 2D/2D heterojunction with enhanced photocatalytic degradation of ibuprofen under visible light irradiation, Appl. Catal. B: Environ. 209 (2017) 285–294.
[19] J. Li, L. Xu, J. He, P. Zhou, L.F. Hu, D.W. Li, B. Wang, The structure feature of novel Cu_2O/e-HTi_2NbO_7 nanocomposite and their enhanced photocatalytic activity, Nano 12 (2017).
[20] W. Zhen, X. Ning, B. Yang, Y. Wu, Z. Li, G. Lu, The enhancement of CdS photocatalytic activity for water splitting via anti-photocorrosion by coating Ni_2P shell and removing nascent formed oxygen with artificial gill, Appl. Catal. B: Environ. 221 (2018) 243–257.
[21] B. Sun, W. Zhou, H. Li, L. Ren, P. Qiao, F. Xiao, L. Wang, B. Jiang, H. Fu, Magnetic Fe_2O_3/mesoporous black TiO_2 hollow sphere heterojunctions with wide-spectrum response and magnetic separation, Appl. Catal. B: Environ. 221 (2018) 235–242.
[22] B. Shao, X. Liu, Z. Liu, G. Zeng, Q. Liang, C. Liang, Y. Cheng, W. Zhang, Y. Liu, S. Gong, A novel double Z-scheme photocatalyst Ag_3PO_4/Bi_2S_3/Bi_2O_3 with enhanced visible-light photocatalytic performance for antibiotic degradation, Chem. Eng. J. 368 (2019) 730–745.
[23] L. Tang, C. Feng, Y. Deng, G. Zeng, J. Wang, Y. Liu, H. Feng, J. Wang, Enhanced photocatalytic activity of ternary Ag/g-C_3N_4/$NaTaO_3$ photocatalysts under wide spectrum light radiation: the high potential band protection mechanism, Appl. Catal. B: Environ. 230 (2018) 102–114.
[24] J. Wang, L. Tang, G. Zeng, Y. Liu, Y. Zhou, Y. Deng, J. Wang, B. Peng, Plasmonic Bi metal deposition and g-C_3N_4 coating on Bi_2WO_6 microspheres for efficient visible-light photocatalysis, ACS Sustain. Chem. Eng. 5 (2017) 1062–1072.
[25] H. Wang, H. Chen, Y. Wang, Y.-K. Lyu, Performance and mechanism comparison of manganese oxides at different valence states for catalytic oxidation of NO, Chem. Eng. J. 361 (2019) 1161–1172.
[26] Y. Deng, L. Tang, C. Feng, G. Zeng, Z. Chen, J. Wang, H. Feng, B. Peng, Y. Liu, Y. Zhou, Insight into the dual-channel charge-carrier transfer path for nonmetal plasmonic tungsten oxide based composites with boosted photocatalytic activity under full-spectrum light, Appl. Catal. B: Environ. 235 (2018) 225–237.
[27] J. Wang, L. Tang, G. Zeng, Y. Deng, H. Dong, Y. Liu, L. Wang, B. Peng, C. Zhang, F. Chen, 0D/2D interface engineering of carbon quantum dots modified Bi_2WO_6 ultrathin nanosheets with enhanced photoactivity for full spectrum light utilization and mechanism insight, Appl. Catal. B: Environ. 222 (2018) 115–123.
[28] L. Tang, Y. Liu, J. Wang, G. Zeng, Y. Deng, H. Dong, H. Feng, J. Wang, B. Peng, Enhanced activation process of persulfate by mesoporous carbon for degradation of aqueous organic pollutants: electron transfer mechanism, Appl. Catal. B: Environ. 231 (2018) 1–10.
[29] C. Feng, Y. Deng, L. Tang, G. Zeng, J. Wang, J. Yu, Y. Liu, B. Peng, H. Feng, J. Wang, Core-shell Ag_2CrO_4/N-GQDs@g-C_3N_4 composites with anti-photocorrosion performance for enhanced full-spectrum-light photocatalytic activities, Appl. Catal. B: Environ. 239 (2018) 525–536.
[30] N. Zhang, L. Wang, H. Wang, R. Cao, J. Wang, F. Bai, H. Fan, Self-assembled one-dimensional porphyrin nanostructures with enhanced photocatalytic hydrogen generation, Nano Lett. 18 (2018) 560–566.
[31] H. Li, Y. Sun, Z.-Y. Yuan, Y.-P. Zhu, T.-Y. Ma, Titanium phosphonate based metal-organic frameworks with hierarchical porosity for enhanced photocatalytic hydrogen evolution, Angew. Chem. Int. Ed. 57 (2018) 3222–3227.

[32] H. Arandiyan, H. Dai, J. Deng, Y. Liu, B. Bai, Y. Wang, X. Li, S. Xie, J. Li, Three-dimensionally ordered macroporous $La_{0.6}Sr_{0.4}MnO_3$ with high surface areas: active catalysts for the combustion of methane, J. Catal. 307 (2013) 327–339.

[33] M.E.L.C.T. Kresge, W.J. Roth, J.C. Vartuli, J.S. Beck, Ordered mesoporous molecular sieves synthesized by a liquid-crystal template mechanism, Nature 359 (1992) 710–712.

[34] H. Fujii, M. Ohtaki, K. Eguchi, Synthesis and photocatalytic activity of lamellar titanium oxide formed by surfactant bilayer templating, J. Am. Chem. Soc. 120 (1998) 6832–6833.

[35] P.N. Trikalitis, K.K. Rangan, T. Bakas, M.G. Kanatzidis, Varied pore organization in mesostructured semiconductors based on the $[SnSe_4]^{4-}$ anion, Nature 410 (2001) 671–675.

[36] M.S. Bakshi, How surfactants control crystal growth of nanomaterials, Cryst. Growth Des. 16 (2015) 1104–1133.

[37] Y.W. Jun, J.S. Choi, J. Cheon, Shape control of semiconductor and metal oxide nanocrystals through nonhydrolytic colloidal routes, Angew. Chem. Int. Ed. Engl. 45 (2006) 3414–3439.

[38] M.A. Nguyen, N.M. Bedford, Y. Ren, E.M. Zahran, R.C. Goodin, F.F. Chagani, L.G. Bachas, M.R. Knecht, Direct synthetic control over the size, composition, and photocatalytic activity of octahedral copper oxide materials: correlation between surface structure and catalytic functionality, ACS Appl. Mater. Interfaces 7 (2015) 13238–13250.

[39] H.S. Yun, K. Miyazawa, H.S. Zhou, I. Honma, M. Kuwabara, Synthesis of mesoporous thin TiO_2 films with hexagonal pore structures using triblock copolymer templates, Adv. Mater. 13 (2001) 1377–1380.

[40] Y.D.D. Li, X.L.L. Li, R.R.R. He, J. Zhu, Z.X.X. Deng, Artificial lamellar mesostructures to WS_2 nanotubes, J. Am. Chem. Soc. 124 (2002) 1411–1416.

[41] Y. Lei, G. Wang, S. Song, W. Fan, H. Zhang, Synthesis, characterization and assembly of BiOCl nanostructure and their photocatalytic properties, CrystEngComm 11 (2009) 1857–1862.

[42] H. Jiang, H. Dai, X. Meng, K. Ji, L. Zhang, J. Deng, Porous olive-like $BiVO_4$: alcohohydrothermal preparation and excellent visible-light-driven photocatalytic performance for the degradation of phenol, Appl. Catal. B: Environ. 105 (2011) 326–334.

[43] Y. Zhou, Z. Zhao, F. Wang, K. Cao, D.E. Doronkin, F. Dong, J.-D. Grunwaldt, Facile synthesis of surface N-doped $Bi_2O_2CO_3$: origin of visible light photocatalytic activity and in situ DRIFTS studies, J. Hazard. Mater. 307 (2016) 163–172.

[44] Y. Guo, Y. Zhang, N. Tian, H. Huang, Homogeneous {0 0 1}-BiOBr/Bi heterojunctions: facile controllable synthesis and morphology-dependent photocatalytic activity, ACS Sustain. Chem. Eng. 4 (2016) 4003–4012.

[45] T.R. Gordon, M. Cargnello, T. Paik, F. Mangolini, R.T. Weber, P. Fornasiero, C.B. Murray, Nonaqueous synthesis of TiO_2 nanocrystals using TiF_4 to engineer morphology, oxygen vacancy concentration, and photocatalytic activity, J. Am. Chem. Soc. 134 (2012) 6751–6761.

[46] X. Xu, Z. Gao, Z. Cui, Y. Liang, Z. Li, S. Zhu, X. Yang, J. Ma, Synthesis of Cu_2O octadecahedron/TiO_2 quantum dot heterojunctions with high visible light photocatalytic activity and high stability, ACS Appl. Mater. Interfaces 8 (2016) 91–101.

[47] K. Zinovjev, I. Tuñón, Reaction coordinates and transition states in enzymatic catalysis, Wiley Interdiscip. Rev. Comput. Mol. Sci. 8 (2018) e1329.

[48] Y. Su, H. Li, H. Ma, J. Robertson, A. Nathan, Controlling surface termination and facet orientation in Cu_2O nanoparticles for high photocatalytic activity: a combined experimental and density functional theory study, ACS Appl. Mater. Interfaces 9 (2017) 8100–8106.

[49] Y. AlSalka, A. Hakki, J. Schneider, D.W. Bahnemann, Co-catalyst-free photocatalytic hydrogen evolution on TiO_2: synthesis of optimized photocatalyst through statistical material science, Appl. Catal. B: Environ. 238 (2018) 422–433.

[50] R. Guan, X. Yuan, Z. Wu, H. Wang, L. Jiang, Y. Li, G. Zeng, Functionality of surfactants in waste-activated sludge treatment: a review, Sci. Total Environ. 609 (2017) 1433–1442.

[51] C. Trellu, E. Mousset, Y. Pechaud, D. Huguenot, E.D. van Hullebusch, G. Esposito, M.A. Oturan, Removal of hydrophobic organic pollutants from soil washing/flushing solutions: a critical review, J. Hazard. Mater. 306 (2016) 149–174.

[52] M. Cheng, G. Zeng, D. Huang, C. Yang, C. Lai, C. Zhang, Y. Liu, Tween 80 surfactant-enhanced bioremediation: toward a solution to the soil contamination by hydrophobic organic compounds, Crit. Rev. Biotechnol. 38 (2018) 17–30.

[53] X.-Y. Yang, L.-H. Chen, Y. Li, J.C. Rooke, C. Sanchez, B.-L. Su, Hierarchically porous materials: synthesis strategies and structure design, Chem. Soc. Rev. 46 (2017) 481–558.

[54] J.L. Blin, A. Leonard, Z.Y. Yuan, L. Gigot, A. Vantomme, A.K. Cheetham, B.L. Su, Hierarchically mesoporous/macroporous metal oxides templated from polyethylene oxide surfactant assemblies, Angew. Chem. Int. Ed. Engl. 42 (2003) 2872–2875.

[55] M. Sharma, D. Das, A. Baruah, A. Jain, A.K. Ganguli, Design of porous silica supported tantalum oxide hollow spheres showing enhanced photocatalytic activity, Langmuir 30 (2014) 3199–3208.

[56] Y. Zhong, J. Wang, R. Zhang, W. Wei, H. Wang, X. Lu, F. Bai, H. Wu, R. Haddad, H. Fan, Morphology-controlled self-assembly and synthesis of photocatalytic nanocrystals, Nano Lett. 14 (2014) 7175–7179.

[57] N.G. Macedo, A.F. Gouveia, R.A. Roca, M. Assis, L. Gracia, J. Andrés, E.R. Leite, E. Longo, Surfactant-mediated morphology and photocatalytic activity of α-Ag_2WO_4 material, J. Mater. Chem. C 122 (2018) 8667–8679.

[58] F.-L. Li, H.-J. Zhang, Synthesis of hollow sphere and 1D structural materials by sol-gel process, Materials 10 (2017).

[59] Y. Li, J. Shi, Hollow-structured mesoporous materials: chemical synthesis, functionalization and applications, Adv. Mater. 26 (2014) 3176–3205.

[60] Q. Hu, Y. Li, N. Zhao, C. Ning, X. Chen, Facile synthesis of hollow mesoporous bioactive glass sub-micron spheres with a tunable cavity size, Mater. Lett. 134 (2014) 130–133.

[61] J. Sun, G. Chen, J. Wu, H. Dong, G. Xiong, Bismuth vanadate hollow spheres: Bubble template synthesis and enhanced photocatalytic properties for photodegradation, Appl. Catal. B: Environ. 132 (2013) 304–314.

[62] Y. Li, J. Liu, X. Huang, G. Li, Hydrothermal synthesis of Bi_2WO_6 uniform hierarchical microspheres, Cryst. Growth Des. 7 (2007) 1350–1355.

[63] R. Buonsanti, V. Grillo, E. Carlino, C. Giannini, T. Kipp, R. Cingolani, P.D. Cozzoli, Nonhydrolytic synthesis of high-quality anisotropically shaped brookite TiO_2 nanocrystals, J. Am. Chem. Soc. 130 (2008) 11223–11233.

[64] J. Yu, C.-Y. Xu, F.-X. Ma, S.-P. Hu, Y.-W. Zhang, L. Zhen, Monodisperse SnS_2 nanosheets for high-performance photocatalytic hydrogen generation, ACS Appl. Mater. Interfaces 6 (2014) 22370–22377.

[65] H. Yang, X.-L. Wu, M.-H. Cao, Y.-G. Guo, Solvothermal synthesis of $LiFePO_4$ hierarchically dumbbell-like microstructures by nanoplate self-assembly and their application as a cathode material in lithium-ion batteries, J. Phys. Chem. C 113 (2009) 3345–3351.

[66] J. Jiang, Q. Zhang, X. Zhan, F. Chen, A multifunctional gelatin-based aerogel with superior pollutants adsorption, oil/water separation and photocatalytic properties, Chem. Eng. J. 358 (2019) 1539–1551.

[67] M. Li, C. Bian, G. Yang, X. Qiang, Facile fabrication of water-based and non-fluorinated superhydrophobic sponge for efficient separation of immiscible oil/water mixture and water-in-oil emulsion, Chem. Eng. J. 368 (2019) 350–358.

[68] M. Zhu, P. Chen, M. Liu, Ag/AgBr/graphene oxide nanocomposite synthesized via oil/water and water/oil microemulsions: a comparison of sunlight energized plasmonic photocatalytic activity, Langmuir 28 (2012) 3385–3390.

[69] X.-K. Wang, C. Wang, W.-Q. Jiang, W.-L. Guo, J.-G. Wang, Sonochemical synthesis and characterization of Cl-doped TiO_2 and its application in the photodegradation of phthalate ester under visible light irradiation, Chem. Eng. J. 189 (2012) 288–294.

[70] J. Fu, G.Z. Kyzas, Z. Cai, E.A. Deliyanni, W. Liu, D. Zhao, Photocatalytic degradation of phenanthrene by graphite oxide-TiO_2-$Sr(OH)_2$/$SrCO_3$ nanocomposite under solar irradiation: effects of water quality parameters and predictive modeling, Chem. Eng. J. 335 (2018) 290–300.

[71] M. Panahi-Kalamuei, M. Mousavi-Kamazani, M. Salavati-Niasari, S.M. Hosseinpour-Mashkani, A simple sonochemical approach for synthesis of selenium nanostructures and investigation of its light harvesting application, Ultrason. Sonochem. 23 (2015) 246–256.

[72] K. Li, S. Li, J. Zhang, Z. Feng, C. Li, Preparation and stabilization of gamma-Bi_2O_3 photocatalyst by adding surfactant and its photocatalytic performance, Mater. Res. Express 4 (2017).

[73] R.F. Ali, A.H. Nazemi, B.D. Gates, Surfactant controlled growth of niobium oxide nanorods, Cryst. Growth Des. 17 (2017) 4637–4646.

[74] M. Zhu, Z. Li, B. Xiao, Y. Lu, Y. Du, P. Yang, X. Wang, Surfactant assistance in improvement of photocatalytic hydrogen production with the porphyrin non-covalently functionalized graphene nanocomposite, ACS Appl. Mater. Interfaces 5 (2013) 1732–1740.

[75] M. Ge, Y. Li, L. Liu, Z. Zhou, W. Chen, $Bi_2O_3-Bi_2WO_6$ composite microspheres: hydrothermal synthesis and photocatalytic performances, J. Mater. Chem. C 115 (2011) 5220–5225.

[76] P. Guo, P. Chen, M. Liu, One-dimensional porphyrin nanoassemblies assisted via graphene oxide: sheetlike functional surfactant and enhanced photocatalytic behaviors, ACS Appl. Mater. Interfaces 5 (2013) 5336–5345.

[77] F. Petronella, E. Fanizza, G. Mascolo, V. Locaputo, L. Bertinetti, G. Martra, S. Coluccia, A. Agostiano, M.L. Curri, R. Comparelli, Photocatalytic activity of nanocomposite catalyst films based on nanocrystalline metal/semiconductors, J. Mater. Chem. C 115 (2011) 12033–12040.

[78] K. Li, J. Xiong, T. Chen, L. Yan, Y. Dai, D. Song, Y. Lv, Z. Zeng, Preparation of graphene/TiO_2 composites by nonionic surfactant strategy and their simulated sunlight and visible light photocatalytic activity towards representative aqueous POPs degradation, J. Hazard. Mater. 250 (2013) 19–28.

[79] X. Yang, F. Ma, K. Li, Y. Guo, J. Hu, W. Li, M. Huo, Y. Guo, Mixed phase titania nanocomposite codoped with metallic silver and vanadium oxide: new efficient photocatalyst for dye degradation, J. Hazard. Mater. 175 (2010) 429–438.

[80] X.M. Sun, X. Chen, Z.X. Deng, Y.D. Li, A CTAB-assisted hydrothermal orientation growth of ZnO nanorods, Mater. Chem. Phys. 78 (2003) 99–104.

[81] F. Ji, C. Li, J. Zhang, Hydrothermal synthesis of $Li_9Fe_3(P_2O_7)_3(PO_4)_2$ nanoparticles and their photocatalytic properties under visible-light illumination, ACS Appl. Mater. Interfaces 2 (2010) 1674–1678.

[82] N. Zhao, L. Qi, Low-temperature synthesis of star-shaped PbS nanocrystals in aqueous solutions of mixed cationic/anionic surfactants, Adv. Mater. 18 (2006) 359–362.

[83] X. Wang, J.C. Yu, C. Ho, Y. Hou, X. Fu, Photocatalytic activity of a hierarchically macro/mesoporous titania, Langmuir 21 (2005) 2552–2559.

[84] N. Shi, W. Du, X. Jin, Y. Zhang, M. Han, Z. Xu, L. Xie, W. Huang, Surfactant charge mediated shape control of nano- or microscaled coordination polymers: the case of tetrapyridylporphine based metal complex, Cryst. Growth Des. 14 (2014) 1251–1257.

[85] N. Zhao, Y. Wei, N. Sun, Q. Chen, J. Bai, L. Zhou, Y. Qin, M. Li, L. Qi, Controlled synthesis of gold nanobelts and nanocombs in aqueous mixed surfactant solutions, Langmuir 24 (2008) 991–998.

[86] F. Li, Y. Jiang, M. Xia, M. Sun, B. Xue, X. Ren, A high-stability silica-clay composite: synthesis, characterization and combination with TiO_2 as a novel photocatalyst for Azo dye, J. Hazard. Mater. 165 (2009) 1219–1223.

[87] M. Masjedi-Arani, M. Salavati-Niasari, A simple sonochemical approach for

synthesis and characterization of Zn_2SiO_4 nanostructures, Ultrason. Sonochem. 29 (2016) 226–235.
[88] X. Qi, T. Balankura, Y. Zhou, K.A. Fichthorn, How structure-directing agents control nanocrystal shape: polyvinylpyrrolidone-mediated growth of Ag nanocubes, Nano Lett. 15 (2015) 7711–7717.
[89] A. Shimojima, Z. Liu, T. Ohsuna, O. Terasaki, K. Kuroda, Self-assembly of designed oligomeric siloxanes with alkyl chains into silica-based hybrid mesostructures, J. Am. Chem. Soc. 127 (2005) 14108–14116.
[90] Y. Ni, L. Jin, J. Hong, Phase-controllable synthesis of nanosized nickel phosphides and comparison of photocatalytic degradation ability, Nanoscale 3 (2011) 196–200.
[91] R.C. Wadams, L. Fabris, R.A. Vaia, K. Park, Time-dependent susceptibility of the growth of gold nanorods to the addition of a cosurfactant, Chem. Mater. 25 (2013) 4772–4780.
[92] R. Chen, J. Bi, L. Wu, Z. Li, X. Fu, Orthorhombic Bi_2GeO_5 nanobelts: synthesis, characterization, and photocatalytic properties, Cryst. Growth Des. 9 (2009) 1775–1779.
[93] M. Zhu, Y. Wang, D. Meng, X. Qin, G. Diao, Hydrothermal synthesis of hematite nanoparticles and their electrochemical properties, J. Phys. Chem. C 116 (2012) 16276–16285.
[94] M. Zhu, P. Chen, M. Liu, Sunlight-driven plasmonic photocatalysts based on Ag/AgCl nanostructures synthesized via an oil-in-water medium: enhanced catalytic performance by morphology selection, J. Mater. Chem. 21 (2011) 16413–16419.
[95] Y. Chen, D.D. Dionysiou, Bimodal mesoporous TiO_2-P25 composite thick films with high photocatalytic activity and improved structural integrity, Appl. Catal. B: Environ. 80 (2008) 147–155.
[96] D. Ke, T. Peng, L. Ma, P. Cai, K. Dai, Effects of hydrothermal temperature on the microstructures of $BiVO_4$ and its photocatalytic O_2 evolution activity under visible light, Inorg. Chem. 48 (2009) 4685–4691.
[97] H. Choi, E. Stathatos, D.D. Dionysiou, Synthesis of nanocrystalline photocatalytic TiO_2 thin films and particles using sol-gel method modified with nonionic surfactants, Thin Solid Films 510 (2006) 107–114.
[98] U. Schubert, Chemical modification of titanium alkoxides for sol–gel processing, J. Mater. Chem. 15 (2005) 3701.
[99] B. Geng, B. Tao, X. Li, W. Wei, Ni^{2+}/surfactant-assisted route to porous alpha-Fe_2O_3 nanoarchitectures, Nanoscale 4 (2012) 1671–1676.
[100] H. Cheng, W. Wang, B. Huang, Z. Wang, J. Zhan, X. Qin, X. Zhang, Y. Dai, Tailoring AgI nanoparticles for the assembly of AgI/BiOI hierarchical hybrids with size-dependent photocatalytic activities, J. Mater. Chem. A 1 (2013) 7131–7136.
[101] D. Wang, P. Kanhere, M. Li, Q. Tay, Y. Tang, Y. Huang, T.C. Sum, N. Mathews, T. Sritharan, Z. Chen, Improving photocatalytic H_2 evolution of TiO_2 via formation of {0 0 1}–{010} quasi-heterojunctions, J. Mater. Chem. C 117 (2013) 22894–22902.
[102] M. Pelaez, A.A. de la Cruz, E. Stathatos, P. Falaras, D.D. Dionysiou, Visible light-activated N-F-codoped TiO_2 nanoparticles for the photocatalytic degradation of microcystin-LR in water, Catal. Today 144 (2009) 19–25.
[103] B. Tan, H.J. Lehmler, S.M. Vyas, B.L. Knutson, S.E. Rankin, Controlling nanopore size and shape by fluorosurfactant templating of silica, Chem. Mater. 17 (2005) 916–925.
[104] G. Liu, C. Han, M. Pelaez, D. Zhu, S. Liao, V. Likodimos, N. Ioannidis, A.G. Kontos, P. Falaras, P.S.M. Dunlop, J.A. Byrne, D.D. Dionysiou, Synthesis, characterization and photocatalytic evaluation of visible light activated C-doped TiO_2 nanoparticles, Nanotechnology 23 (2012).
[105] K.S. Ranjith, R. Pandian, E. McGlynn, R.T. Rajendra Kumar, Alignment, morphology and defect control of vertically aligned ZnO nanorod array: competition between “surfactant” and “stabilizer” roles of the amine species and its photocatalytic properties, Cryst. Growth Des. 14 (2014) 2873–2879.
[106] C. Ni, P.A. Hassan, E.W. Kaler, Structural characteristics and growth of pentagonal silver nanorods prepared by a surfactant method, Langmuir 21 (2005) 3334–3337.
[107] H. Usui, Surfactant concentration dependence of structure and photocatalytic properties of zinc oxide rods prepared using chemical synthesis in aqueous solutions, J. Colloid Interface Sci. 336 (2009) 667–674.
[108] X. Meng, L. Zhang, H. Dai, Z. Zhao, R. Zhang, Y. Liu, Surfactant-assisted hydrothermal fabrication and visible-light-driven photocatalytic degradation of methylene blue over multiple morphological $BiVO_4$ single-crystallites, Mater. Chem. Phys. 125 (2011) 59–65.
[109] J. Wang, Y. Zhong, L. Wang, N. Zhang, R. Cao, K. Bian, L. Alarid, R.E. Haddad, F. Bai, H. Fan, Morphology-controlled synthesis and metalation of porphyrin nanoparticles with enhanced photocatalytic performance, Nano Lett. 16 (2016) 6523–6528.
[110] S. Mandal, S.K. Nayak, S. Mallampalli, A. Patra, Surfactant-assisted porphyrin based hierarchical nano/micro assemblies and their efficient photocatalytic behavior, ACS Appl. Mater. Interfaces 6 (2014) 130–136.
[111] A.W. Xu, M. Antonietti, H. Cölfen, Y.P. Fang, Uniform hexagonal plates of vaterite $CaCO_3$ mesocrystals formed by biomimetic mineralization, Adv. Funct. Mater. 16 (2006) 903–908.
[112] J. Huang, K. Ding, X. Wang, X. Fu, Nanostructuring cadmium germanate catalysts for photocatalytic oxidation of benzene at ambient conditions, Langmuir 25 (2009) 8313–8319.
[113] J. Huang, K. Ding, Y. Hou, X. Wang, X. Fu, Synthesis and photocatalytic activity of Zn_2GeO_4 nanorods for the degradation of organic pollutants in water, ChemSusChem 1 (2008) 1011–1019.
[114] T. Sreethawong, S. Ngamsinlapasathian, Y. Suzuki, S. Yoshikawa, Nanocrystalline mesoporous Ta_2O_5-based photocatalysts prepared by surfactant-assisted templating sol-gel process for photocatalytic H_2 evolution, J. Mol. Catal. A: Chem. 235 (2005) 1–11.
[115] L. Tian, L. Ye, K. Deng, L. Zan, TiO_2/carbon nanotube hybrid nanostructures: solvothermal synthesis and their visible light photocatalytic activity, J. Solid State Chem. 184 (2011) 1465–1471.
[116] D.S. Selishchev, I.P. Karaseva, V.V. Uvaev, D.V. Kozlov, V.N. Parmon, Effect of preparation method of functionalized textile materials on their photocatalytic activity and stability under UV irradiation, Chem. Eng. J. 224 (2013) 114–120.
[117] N.E. Valderruten, W.F. Pena, A.E. Ramirez, J.E. Rodriguez-Paez, Effect of the synthetic method on the catalytic activity of alumina: epoxidation of cyclohexene, Mater. Res. Bull. 62 (2015) 80–87.
[118] T. Zieba, M. Kapelko, A. Szumny, Effect of preparation method on the properties of potato starch acetates with an equal degree of substitution, Carbohydr. Polym. 94 (2013) 193–198.
[119] L. Liu, S. Ouyang, J. Ye, Gold-nanorod-photosensitized titanium dioxide with wide-range visible-light harvesting based on localized surface plasmon resonance, Angew. Chem. Int. Ed. 52 (2013) 6689–6693.
[120] S. Sakulkhaemaruethai, S. Pavasupree, Y. Suzuki, S. Yoshikawa, Photocatalytic activity of titania nanocrystals prepared by surfactant-assisted templating method – effect of calcination conditions, Mater. Lett. 59 (2005) 2965–2968.
[121] A. Alagarasi, P.U. Rajalakshmi, K. Shanthi, P. Selvam, Ordered mesoporous nanocrystalline titania: a promising new class of photocatalyic materials, Catal. Today 309 (2018) 202–211.
[122] S.K. Batabyal, S.E. Lu, J.J. Vittal, Synthesis, characterization, and photocatalytic properties of In_2S_3, $ZnIn_2S_4$, and $CdIn_2S_4$ nanocrystals, Cryst. Growth Des. 16 (2016) 2231–2238.
[123] U. Cernigoj, U.L. Stangar, P. Trebse, U.O. Krasovec, S. Gross, Photocatalytically active TiO_2 thin films produced by surfactant-assisted sol-gel processing, Thin Solid Films 495 (2006) 327–332.
[124] Y. Zhang, H. Wu, J. Zhang, H. Wang, W. Lu, Enhanced photodegradation of pentachlorophenol by single and mixed cationic and nonionic surfactants, J. Hazard. Mater. 221 (2012) 92–99.
[125] J.W. Liu, R. Han, H.T. Wang, Y. Zhao, Z. Chu, H.Y. Wu, Photoassisted degradation of pentachlorophenol in a simulated soil washing system containing nonionic surfactant Triton X-100 with La–B codoped TiO_2 under visible and solar light irradiation, Appl. Catal. B: Environ. 103 (2011) 470–478.
[126] J.-C. Lin, C.-Y. Hu, S.-L. Lo, Effect of surfactants on the degradation of perfluorooctanoic acid (PFOA) by ultrasonic (US) treatment, Ultrason. Sonochem. 28 (2016) 130–135.
[127] L. Tang, J. Wang, G. Zeng, Y. Liu, Y. Deng, Y. Zhou, J. Tang, J. Wang, Z. Guo, Enhanced photocatalytic degradation of norfloxacin in aqueous Bi_2WO_6 dispersions containing nonionic surfactant under visible light irradiation, J. Hazard. Mater. 306 (2016) 295–304.
[128] X. Liang, C. Guo, C. Liao, S. Liu, L.Y. Wick, D. Peng, X. Yi, G. Lu, H. Yin, Z. Lin, Z. Dang, Drivers and applications of integrated clean-up technologies for surfactant-enhanced remediation of environments contaminated with polycyclic aromatic hydrocarbons (PAHs), Environ. Pollut. 225 (2017) 129–140.
[129] Y. Zhang, J.W.C. Wong, P. Liu, M. Yuan, Heterogeneous photocatalytic degradation of phenanthrene in surfactant solution containing TiO_2 particles, J. Hazard. Mater. 191 (2011) 136–143.
[130] K. Zhang, J. Liang, S. Wang, J. Liu, K. Ren, X. Zheng, H. Luo, Y. Peng, X. Zou, X. Bo, J. Li, X. Yu, BiOCl sub-microcrystals induced by citric acid and their high photocatalytic activities, Cryst. Growth Des. 12 (2012) 793–803.
[131] Y. Huo, J. Zhang, M. Miao, Y. Jin, Solvothermal synthesis of flower-like BiOBr microspheres with highly visible-light photocatalytic performances, Appl. Catal. B: Environ. 111 (2012) 334–341.
[132] H. Choi, A.C. Sofranko, D.D. Dionysiou, Nanocrystalline TiO_2 photocatalytic membranes with a hierarchical mesoporous multilayer structure: synthesis, characterization, and multifunction, Adv. Funct. Mater. 16 (2006) 1067–1074.
[133] H. Choi, E. Stathatos, D.D. Dionysiou, Sol-gel preparation of mesoporous photocatalytic TiO_2 films and TiO_2/Al_2O_3 composite membranes for environmental applications, Appl. Catal. B: Environ. 63 (2006) 60–67.
[134] C. Han, M. Pelaez, V. Likodimos, A.G. Kontos, P. Falaras, K. O'Shea, D.D. Dionysiou, Innovative visible light-activated sulfur doped TiO_2 films for water treatment, Appl. Catal. B: Environ. 107 (2011) 77–87.
[135] E. Grabowska, Selected perovskite oxides: characterization, preparation and photocatalytic properties—a review, Appl. Catal. B: Environ. 186 (2016) 97–126.
[136] J. Song, X. Wang, J. Ma, X. Wang, J. Wang, S. Xia, J. Zhao, Removal of Microcystis aeruginosa and microcystin-LR using a graphitic-C_3N_4/TiO_2 floating photocatalyst under visible light irradiation, Chem. Eng. J. 348 (2018) 380–388.
[137] H. Hao, J. Zhang, The study of iron(III) and nitrogen co-doped mesoporous TiO_2 photocatalysts: synthesis, characterization and activity, Microporous Mesoporous Mater. 121 (2009) 52–57.
[138] M. Jia, X. Hu, S. Wang, Y. Huang, L. Song, Photocatalytic properties of hierarchical BiOXs obtained via an ethanol-assisted solvothermal process, J. Environ. Sci. 35 (2015) 172–180.
[139] H. Choi, M.G. Antoniou, M. Pelaez, A.A. De la Cruz, J.A. Shoemaker, D.D. Dionysiou, Mesoporous nitrogen-doped TiO_2 for the photocatalytic destruction of the cyanobacterial toxin microcystin-LR under visible light irradiation, Environ. Sci. Technol. 41 (2007) 7530–7535.
[140] P. Bouras, E. Stathatos, P. Lianos, Pure versus metal-ion-doped nanocrystalline titania for photocatalysis, Appl. Catal. B: Environ. 73 (2007) 51–59.
[141] J. Cai, X. Wu, S. Li, F. Zheng, L. Zhu, Z. Lai, Synergistic effect of double-shelled and sandwiched TiO_2@Au@C hollow spheres with enhanced visible-light-driven photocatalytic activity, ACS Appl. Mater. Interfaces 7 (2015) 3764–3772.
[142] J. Wang, T. Tsuzuki, L. Sun, X. Wang, Reverse microemulsion-mediated synthesis of SiO_2-coated ZnO composite nanoparticles: multiple cores with tunable shell thickness, ACS Appl. Mater. Interfaces 2 (2010) 957–960.

[143] Z. Li, B. Gao, G.Z. Chen, R. Mokaya, S. Sotiropoulos, G.L. Puma, Carbon nanotube/titanium dioxide (CNT/TiO_2) core-shell nanocomposites with tailored shell thickness, CNT content and photocatalytic/photoelectrocatalytic properties, Appl. Catal. B: Environ. 110 (2011) 50–57.
[144] G. Yoon, D.-H. Kim, I. Park, D. Chang, B. Kim, B. Lee, K. Oh, K. Kang, Using first-principles calculations for the advancement of materials for rechargeable batteries, Adv. Funct. Mater. 1702887 (2017).
[145] D. Wang, Z.-P. Liu, W.-M. Yang, Proton-promoted electron transfer in photocatalysis: key step for photocatalytic hydrogen evolution on metal/titania composites, ACS Catal. 7 (2017) 2744–2752.
[146] Z. Liu, Y. Liu, G. Zeng, B. Shao, M. Chen, Z. Li, Y. Jiang, Y. Liu, Y. Zhang, H. Zhong, Application of molecular docking for the degradation of organic pollutants in the environmental remediation: a review, Chemosphere 203 (2018) 139–150.
[147] Y. Liu, Z. Liu, G. Zeng, M. Chen, Y. Jiang, B. Shao, Z. Li, Y. Liu, Effect of surfactants on the interaction of phenol with laccase: molecular docking and molecular dynamics simulation studies, J. Hazard. Mater. 357 (2018) 10–18.
[148] Y. Zhao, T. Yu, X. Tan, C. Xie, S. Wang, SDS-assisted solvothermal synthesis of rose-like BiOBr partially enclosed by 111 facets and enhanced visible-light photocatalytic activity, Dalton Trans. 44 (2015) 20475–20483.
[149] H. Jiang, X. Meng, H. Dai, J. Deng, Y. Liu, L. Zhang, Z. Zhao, R. Zhang, High-performance porous spherical or octapod-like single-crystalline $BiVO_4$ photocatalysts for the removal of phenol and methylene blue under visible-light illumination, J. Hazard. Mater. 217 (2012) 92–99.
[150] P. Lin, Y. Cong, C. Sun, B. Zhang, Non-covalent modification of reduced graphene oxide by a chiral liquid crystalline surfactant, Nanoscale 8 (2016) 2403–2411.
[151] H. Bantawal, U.S. Shenoy, D.K. Bhat, Tuning the photocatalytic activity of $SrTiO_3$ by varying the Sr/Ti ratio: unusual effect of viscosity of the synthesis medium, J. Phys. Chem. C 122 (2018) 20027–20033.
[152] J. Kim, L.J. Cote, F. Kim, W. Yuan, K.R. Shull, J. Huang, Graphene oxide sheets at interfaces, J. Am. Chem. Soc. 132 (2010) 8180.
[153] O.V. Makarova, T. Rajh, M.C. Thurnauer, A. Martin, P.A. Kemme, D. Cropek, Surface modification of TiO_2 nanoparticles for photochemical reduction of nitrobenzene, Environ. Sci. Technol. 34 (2000) 4797–4803.
[154] Z. Liu, B. Shao, G. Zeng, M. Chen, Z. Li, Y. Liu, Y. Jiang, H. Zhong, Y. Liu, M. Yan, Effects of rhamnolipids on the removal of 2,4,2,4-tetrabrominated biphenyl ether (BDE-47) by Phanerochaete chrysosporium analyzed with a combined approach of experiments and molecular docking, Chemosphere 210 (2018) 922–930.
[155] B. Shao, Z. Liu, H. Zhong, G. Zeng, G. Liu, M. Yu, Y. Liu, X. Yang, Z. Li, Z. Fang, J. Zhang, C. Zhao, Effects of rhamnolipids on microorganism characteristics and applications in composting: a review, Microbiol. Res. 200 (2017) 33–44.
[156] M. Dong, Q. Lin, H. Sun, D. Chen, T. Zhang, Q. Wu, S. Li, Synthesis of cerium molybdate hierarchical architectures and their novel photocatalytic and adsorption performances, Cryst. Growth Des. 11 (2011) 5002–5009.
[157] M.B. Tahir, M. Sagir, K. Shahzad, Removal of acetylsalicylate and methyl-theobromine from aqueous environment using nano-photocatalyst WO_3-TiO_2@g-C_3N_4 composite, J. Hazard. Mater. 363 (2019) 205–213.
[158] X. Lu, W. Che, X. Hu, Y. Wang, A. Zhang, F. Deng, S. Luo, D.D. Dionysiou, The facile fabrication of novel visible-light-driven Z-scheme $CuInS_2$/Bi_2WO_6 heterojunction with intimate interface contact by in situ hydrothermal growth strategy for extraordinary photocatalytic performance, Chem. Eng. J. 356 (2019) 819–829.
[159] J. Bolobajev, M. Kasle, K. Kreek, M. Kulp, M. Koel, A. Goib, Metal-doped organic aerogels for photocatalytic degradation of trimethoprim, Chem. Eng. J. 357 (2019) 120–128.
[160] Y. Yang, Z. Zeng, C. Zhang, D. Huang, G. Zeng, R. Xiao, C. Lai, C. Zhou, H. Guo, W. Xue, M. Cheng, W. Wang, J. Wang, Construction of iodine vacancy-rich BiOI/Ag@AgI Z-scheme heterojunction photocatalysts for visible-light-driven tetracycline degradation: transformation pathways and mechanism insight, Chem. Eng. J. 349 (2018) 808–821.
[161] G. Di, Z. Zhu, Q. Huang, H. Zhang, J. Zhu, Y. Qiu, D. Yin, J. Zhao, Targeted modulation of g-C_3N_4 photocatalytic performance for pharmaceutical pollutants in water using ZnFe-LDH derived mixed metal oxides: structure-activity and mechanism, Sci. Total Environ. 650 (2019) 1112–1121.
[162] D. Mao, S. Ding, L. Meng, Y. Dai, C. Sun, S. Yang, H. He, One-pot microemulsion-mediated synthesis of Bi-rich $Bi4O_5Br_2$ with controllable morphologies and excellent visible-light photocatalytic removal of pollutants, Appl. Catal. B: Environ. 207 (2017) 153–165.
[163] R.K. Singh, L. Philip, S. Ramanujam, Continuous flow pulse corona discharge reactor for the tertiary treatment of drinking water: insights on disinfection and emerging contaminants removal, Chem. Eng. J. 355 (2019) 269–278.
[164] O. Gimeno, J.F. Garcia-Araya, F.J. Beltran, F.J. Rivas, A. Espejo, Removal of emerging contaminants from a primary effluent of municipal wastewater by means of sequential biological degradation-solar photocatalytic oxidation processes, Chem. Eng. J. 290 (2016) 12–20.
[165] D.V.S. Merkulov, V.N. Despotovic, N.D. Banic, S.J. Armakovic, N.L. Fincur, M.J. Lazarevic, D.D. Cetojevic-Simin, D.Z. Orcic, M.B. Radoicic, Z.V. Saponjic, M.I. Comor, B.F. Abramovic, Photocatalytic decomposition of selected biologically active compounds in environmental waters using TiO_2/polyaniline nanocomposites: kinetics, toxicity and intermediates assessment, Environ. Pollut. 239 (2018) 457–465.
[166] O. Ojajuni, S. Holder, G. Cavalli, J. Lee, D.P. Saroj, Rejection of caffeine and carbamazepine by surface-coated PVDF hollow-fiber membrane system, Ind. Eng. Chem. Res. 55 (2016).
[167] L.E. De, S. Chiron, S. Kouras-Hadef, C. Richard, M. Minella, V. Maurino, C. Minero, D. Vione, Photochemical fate of carbamazepine in surface freshwaters: laboratory measures and modeling, Environ. Sci. Technol. 46 (2012) 8164.
[168] J.P. Simon, P.S. Evan, Natural remedies for non-steroidal anti-inflammatory drug-induced toxicity, J. Appl. Toxicol. 37 (2016) 71–83.
[169] D.A. Solis-Casados, L. Escobar-Alarcon, L.M. Gomez-Olivan, E. Haro-Poniatowski, T. Klimova, Photodegradation of pharmaceutical drugs using Sn-modified TiO_2 powders under visible light irradiation, Fuel 198 (2017) 3–10.
[170] M.V.P. Sharma, V.D. Kumari, M. Subrahmanyam, TiO_2 supported over porous silica photocatalysts for pesticide degradation using solar light: Part 2. Silica prepared using acrylic acid emulsion, J. Hazard. Mater. 175 (2010) 1101–1105.
[171] S. Perveen, M.A. Farrukh, $Ti_{0.85}Sn_{0.15}O_2$ nanocomposite: an efficient semiconductor photocatalyst for degradation of pesticides under solar light, J. Mater. Sci. Mater. Electron. 29 (2018) 3219–3230.
[172] J.L. Gong, B. Wang, G.M. Zeng, C.P. Yang, C.G. Niu, Q.Y. Niu, W.J. Zhou, Y. Liang, Removal of cationic dyes from aqueous solution using magnetic multi-wall carbon nanotube nanocomposite as adsorbent, J. Hazard. Mater. 164 (2009) 1517–1522.
[173] K. He, G.Q. Chen, G.M. Zeng, A.W. Chen, Z.Z. Huang, J.B. Shi, T.T. Huang, M. Peng, L. Hu, Three-dimensional graphene supported catalysts for organic dyes degradation, Appl. Catal. B: Environ. 228 (2018) 19–28.
[174] S. Krejcikova, L. Matejova, K. Koci, L. Obalova, Z. Matej, L. Capek, O. Solcova, Preparation and characterization of Ag-doped crystalline titania for photocatalysis applications, Appl. Catal. B: Environ. 111 (2012) 119–125.
[175] J.-M. Wu, Y. Chen, L. Pan, P. Wang, Y. Cui, D. Kong, L. Wang, X. Zhang, J.-J. Zou, Multi-layer monoclinic $BiVO_4$ with oxygen vacancies and V^{4+} species for highly efficient visible-light photoelectrochemical applications, Appl. Catal. B: Environ. 221 (2018) 187–195.
[176] M. Ou, S. Wan, Q. Zhong, S. Zhang, Y. Song, L. Guo, W. Cai, Y. Xu, Hierarchical Z-scheme photocatalyst of g-C_3N_4@Ag/$BiVO_4$ (0 4 0) with enhanced visible-light-induced photocatalytic oxidation performance, Appl. Catal. B: Environ. 221 (2018) 97–107.
[177] D. Mao, J. Yuan, X. Qu, C. Sun, S. Yang, H. He, Size tunable Bi_3O_4Br hierarchical hollow spheres assembled with {0 0 1}-facets exposed nanosheets for robust photocatalysis against phenolic pollutants, J. Catal. 369 (2019) 209–221.
[178] J.-A. Park, B. Yang, J.-H. Kim, J.-W. Choi, H.-D. Park, S.-H. Lee, Removal of microcystin-LR using UV-assisted advanced oxidation processes and optimization of photo-Fenton-like process for treating Nak-Dong River water, South Korea, Chem. Eng. J. 348 (2018) 125–134.
[179] A. Karci, E.M. Wurtzler, A.A. de la Cruz, D. Wendell, D.D. Dionysiou, Solar photo-Fenton treatment of microcystin-LR in aqueous environment: transformation products and toxicity in different water matrices, J. Hazard. Mater. 349 (2018) 282–292.
[180] M.G. Antoniou, P.A. Nicolaou, J.A. Shoemaker, A.A. de la Cruz, D.D. Dionysiou, Impact of the morphological properties of thin TiO_2 photocatalytic films on the detoxification of water contaminated with the cyanotoxin, microcystin-LR, Appl. Catal. B: Environ. 91 (2009) 165–173.
[181] G. Liu, C. Han, M. Pelaez, D. Zhu, S. Liao, V. Likodimos, A.G. Kontos, P. Falaras, D.D. Dionysiou, Enhanced visible light photocatalytic activity of C-N-codoped TiO_2 films for the degradation of microcystin-LR, J. Mol. Catal. A: Chem. 372 (2013) 58–65.
[182] H. Choi, E. Stathatos, D.D. Dionysiou, Photocatalytic TiO_2 films and membranes for the development of efficient wastewater treatment and reuse systems, Desalination 202 (2007) 199–206.
[183] S.M. Hassan, A.I. Ahmed, M.A. Mannaa, Structural, photocatalytic, biological and catalytic properties of SnO_2/TiO_2 nanoparticles, Ceram. Int. 44 (2018) 6201–6211.
[184] A. Jose, K.R.S. Devi, D. Pinheiro, S.L. Narayana, Electrochemical synthesis, photodegradation and antibacterial properties of PEG capped zinc oxide nanoparticles, J. Photochem. Photobiol. B: Biol. 187 (2018) 25–34.
[185] B. Xi, X. Chu, J. Hu, C.S. Bhatia, A.J. Danner, H. Yang, Preparation of Ag/TiO_2/SiO_2 films via photo-assisted deposition and adsorptive self-assembly for catalytic bactericidal application, Appl. Surf. Sci. 311 (2014) 582–592.
[186] Y. Li, F. Zhou, Z. Zhu, F. Wu, Inactivating marine microorganisms for photoelectrocatalysis by $ZnWO_4$ electrode obtained by surfactant-assisted synthesis, Appl. Surf. Sci. 467 (2019) 819–824.
[187] Y. Deng, L. Tang, G. Zeng, Z. Zhu, M. Yan, Y. Zhou, J. Wang, Y. Liu, J. Wang, Insight into highly efficient simultaneous photocatalytic removal of Cr(VI) and 2,4-dicloropheno under visible light irradiation by phosphorus doped porous ultrathin g-C_3N_4 nanosheets from aqueous media: performance and reaction mechanism, Appl. Catal. B: Environ. 203 (2017) 343–354.
[188] X. Tang, G. Zeng, C. Fan, M. Zhou, L. Tang, J. Zhu, J. Wan, D. Huang, M. Chen, P. Xu, C. Zhang, Y. Lu, W. Xiong, Chromosomal expression of CadR on Pseudomonas aeruginosa for the removal of Cd(II) from aqueous solutions, Sci. Total Environ. 636 (2018) 1355–1361.
[189] T. Mishra, J. Hait, N. Aman, R.K. Jana, S. Chakravarty, Effect of UV and visible light on photocatalytic reduction of lead and cadmium over titania based binary oxide materials, J. Colloid Interface Sci. 316 (2007) 80–84.
[190] C. Zheng, L. Xiao, R. Qu, S. Liu, Q. Xin, P. Ji, H. Song, W. Wu, X. Gao, Numerical simulation of selective catalytic reduction of NO and SO_2 oxidation in monolith catalyst, Chem. Eng. J. 361 (2019) 874–884.
[191] Y. Yu, C. Chen, M. Ma, M. Douthwaite, C. He, J. Miao, J. Chen, C. Li, SO_2 promoted in situ recovery of thermally deactivated $Fe_2(SO_4)_3$/TiO_2 NH_3-SCR catalysts: from experimental work to theoretical study, Chem. Eng. J. 361 (2019) 820–829.
[192] Z. Shayegan, C.-S. Lee, F. Haghighat, TiO_2 photocatalyst for removal of volatile organic compounds in gas phase – a review, Chem. Eng. J. 334 (2018) 2408–2439.
[193] P. Yang, J. Li, L. Bao, X. Zhou, X. Zhang, S. Fan, Z. Chen, S. Zuo, C. Qi, Adsorption/catalytic combustion of toxic 1,2-dichloroethane on multifunctional Nb_2O_5-TiO_2 composite metal oxides, Chem. Eng. J. 361 (2019) 1400–1410.
[194] X. Yao, N. Jiang, J. Li, N. Lu, K. Shang, Y. Wu, An improved corona discharge ignited by oxide cathodes with high secondary electron emission for toluene

degradation, Chem. Eng. J. 362 (2019) 339–348.
[195] X. Wang, F. Han, X. Wei, X. Wang, Microstructure and photocatalytic activity of mesoporous TiO_2 film coated on an aluminum foam, Mater. Lett. 64 (2010) 1985–1988.
[196] A. Zhang, J. Zhang, Characterization of visible-light-driven $BiVO_4$ photocatalysts synthesized via a surfactant-assisted hydrothermal method, Spectrochim. Acta Part A: Mol. Biomol. Spectrosc. 73 (2009) 336–341.
[197] D.L. Liao, B.Q. Liao, Shape, size and photocatalytic activity control of TiO_2 nanoparticles with surfactants, J. Photochem. Photobiol. C: Photochem. Rev. 187 (2007) 363–369.
[198] F. Soofivand, F. Mohandes, M. Salavati-Niasari, Silver chromate and silver dichromate nanostructures: sonochemical synthesis, characterization, and photocatalytic properties, Mater. Res. Bull. 48 (2013) 2084–2094.
[199] S. Shen, L. Zhao, L. Guo, Crystallite, optical and photocatalytic properties of visible-light-driven $ZnIn_2S_4$ photocatalysts synthesized via a surfactant-assisted hydrothermal method, Mater. Res. Bull. 44 (2009) 100–105.
[200] L. Chen, R. Huang, M. Xiong, Q. Yuan, J. He, J. Jia, M.-Y. Yao, S.-L. Luo, C.-T. Au, S.-F. Yin, Room-temperature synthesis of flower-like BiOX (X = Cl, Br, I) hierarchical structures and their visible-light photocatalytic activity, Inorg. Chem. 52 (2013) 11118–11125.
[201] J. Yuenyongsuwan, N. Nithiyakorn, P. Sabkird, E.A. O'Rear, T. Pongprayoon, Surfactant effect on phase-controlled synthesis and photocatalyst property of TiO_2 nanoparticles, Mater. Chem. Phys. 214 (2018) 330–336.
[202] N. Dinh Cung Tien, L. Zhu, Q. Zhang, K.Y. Cho, W.-C. Oh, A new synergetic mesoporous silica combined to CdSe-graphene nanocomposite for dye degradation and hydrogen evolution in visible light, Mater. Res. Bull. 107 (2018) 14–27.
[203] H. Feng, M.-H. Zhang, L.E. Yu, Phosphorus-doped TiO_2 catalysts with stable anatase-brookite biphase structure: synthesis and photocatalytic performance, J. Nanosci. Nanotechnol. 13 (2013) 4981–4989.
[204] N. Dinh Cung Tien, K.Y. Cho, C.-H. Jung, W.-C. Oh, Photocatalytic activities of contaminants by Bi_2WO_6-graphene composites decorated with mesoporous silica, J. Alloys Compd. 766 (2018) 477–487.
[205] L.D.L. Miranda, C.R. Bellato, J.L. Milagres, L.G. Moura, A.H. Mounteer, M.F. de Almeida, Hydrotalcite-TiO_2 magnetic iron oxide intercalated with the anionic surfactant dodecylsulfate in the photocatalytic degradation of methylene blue dye, J. Environ. Manage. 156 (2015) 225–235.
[206] Y. Zhang, N. Zhang, Z.-R. Tang, Y.-J. Xu, Graphene oxide as a surfactant and support for in-situ synthesis of Au–Pd nanoalloys with improved visible light photocatalytic activity, J. Mater. Chem. C 118 (2014) 5299–5308.
[207] C. Xu, H. Wu, F.L. Gu, Efficient adsorption and photocatalytic degradation of Rhodamine B under visible light irradiation over BiOBr/montmorillonite composites, J. Hazard. Mater. 275 (2014) 185–192.
[208] T. Sreethawong, S. Ngamsinlapasathian, S. Yoshikawa, Photochemically deposited nano-Ag/sol-gel TiO_2-In_2O_3 mixed oxide mesoporous-assembled nanocrystals for photocatalytic dye degradation, J. Colloid Interface Sci. 421 (2014) 191–198.
[209] M.J. Muñoz-Batista, M.N. Gómez-Cerezo, A. Kubacka, D. Tudela, M. Fernández-García, Role of interface contact in CeO_2–TiO_2 photocatalytic composite materials, ACS Catal. 4 (2014) 63–72.
[210] E. DeOliveira, C.R. Neri, A.O. Ribeiro, V.S. Garcia, L.L. Costa, A.O. Moura, A.G.S. Prado, O.A. Serra, Y. Iamamoto, Hexagonal mesoporous silica modified with copper phthalocyanine as a photocatalyst for pesticide 2,4-dichlorophenoxiacetic acid degradation, J. Colloid Interface Sci. 323 (2008) 98–104.
[211] S. Yin, H. Tian, Z. Ren, X. Wei, C. Chao, J. Pei, X. Li, G. Xu, G. Shen, G. Han, Octahedral-shaped perovskite nanocrystals and their visible-light photocatalytic activity, Chem. Commun. 50 (2014) 6027–6030.
[212] M. Aslam, M.T. Qamar, A.U. Rehman, M.T. Soomro, S. Ali, I.M.I. Ismail, A. Hameed, The evaluation of the photocatalytic activity of magnetic and non-magnetic polymorphs of Fe_2O_3 in natural sunlight exposure: a comparison of photocatalytic activity, Appl. Surf. Sci. 451 (2018) 128–140.
[213] K. Inumaru, M. Yasui, T. Kasahara, K. Yamaguchi, A. Yasuda, S. Yamanaka, Nanocomposites of crystalline TiO_2 particles and mesoporous silica: molecular selective photocatalysis tuned by controlling pore size and structure, J. Mater. Chem. 21 (2011) 12117.
[214] X. Zhou, C. Hu, X. Hu, T. Peng, J. Qu, Plasmon-assisted degradation of toxic pollutants with Ag-AgBr/Al_2O_3 under visible-light irradiation, J. Phys. Chem. C 114 (2010) 2746–2750.
[215] S.M. El-Sheikh, G. Zhang, H.M. El-Hosainy, A.A. Ismail, K.E. O'Shea, P. Falaras, A.G. Kontos, D.D. Dionysiou, High performance sulfur, nitrogen and carbon doped mesoporous anatase-brookite TiO_2 photocatalyst for the removal of microcystin-LR under visible light irradiation, J. Hazard. Mater. 280 (2014) 723–733.